

Mass-conserving subglacial hydrology in the Parallel Ice Sheet Model

E. Bueler¹ and W. Van Pelt²

¹Department of Mathematics and Statistics, University of Alaska Fairbanks, Alaska, USA

²Institute for Marine and Atmospheric Research Utrecht, The Netherlands^a

^aCurrent address: Norwegian Polar Institute, Tromsø, Norway

Correspondence to: Ed Bueler (elbueler@alaska.edu)

Abstract. We describe and test a distributed subglacial hydrology model which combines pressurized, plastic till with a system of water-filled, linked cavities which open through sliding-generated cavitation and close through ice creep. The addition of this sub-model to the Parallel Ice Sheet Model accomplishes three specific goals: (1) conservation of the mass of two-phase (solid/liquid) water in the ice sheet, (2) simulation of spatially- and temporally-variable basal shear stress from physical mechanisms based on a minimal number of free parameters, and (3) convergence under two-dimensional grid refinement of the subglacial water amount and pressure. The model is a common generalization of several others: (i) the undrained plastic bed model of Tulaczyk et al. (2000b), (ii) a standard “routing” model used for identifying locations of subglacial lakes, (iii) the lumped englacial/subglacial model of (Bartholomäus et al., 2011), and (iv) the elliptic-pressure-equation model of Schoof et al. (2012). We use englacial porosity as a regularization, and we preserve physical bounds on the pressure. In steady state the model generates a local functional relationship between water amount and pressure. We construct an exact solution of the coupled, steady equations which is used for verification of our explicit time-stepping, parallel numerical implementation. We demonstrate the model at scale by five year simulations of the entire Greenland ice sheet at 2 km horizontal resolution, with one million nodes in the hydrology grid.

1 Introduction

Any reasonable dynamical model of the liquid water underneath and within a glacier or ice sheet has at least these two elements: the mass of the water is conserved and the water

flows from high to low values of the modeled hydraulic potential. Beyond that there are many variations considered in the literature. Modeled aquifer geometry might be a system of linked cavities (Kamb, 1987), conduits (Nye, 1976), or a sheet (Creyts and Schoof, 2009). Geometry evolution processes might include the opening of cavities by sliding of the overlying ice past bedrock bumps (Schoof, 2005), the creation of cavities by interaction of the ice with deformable sediment (Schoof, 2007), closure of cavities and conduits by creep (Hewitt, 2011), or melt on the walls of cavities and conduits which causes them to open (Clarke, 2005). Water could move in a macro-porous englacial system (Bartholomäus et al., 2011; Harper et al., 2010) or it could be stored in a porous till (Tulaczyk et al., 2000a).

Successful models have combined subsets of these different morphologies and processes—for examples see Flowers and Clarke (2002a); Hewitt (2013); van der Wel et al. (2013); Werder et al. (2013); de Fleurian et al. (2014). It is not, however, always true that adding more processes makes a better model. Especially when used to understand variations in ice flow and sliding, which is a goal here, the completeness of the modeled processes in a hydrology model should be balanced against the number of uncertain model parameters and the ultimate availability of observations with which to constrain these parameters.

This paper describes a carefully-selected model for a distributed system of linked subglacial cavities, with additional storage of water in the pore spaces of subglacial till. The mass conservation equation in our model describes the evolution of the sum of the transportable water in the distributed system and the water stored in the till. Water in excess of the capacity of the till passes into the transport system, and in this sense the model could be called a “drained-and-conserved

65 plastic bed” model in contrast to the “undrained plastic bed” 120 model of Tulaczyk et al. (2000b).

The goals of the current work are the selection, implementation, verification, and practical demonstration of a two-dimensional subglacial hydrology model. This subglacial component is an ice-dynamics-coupled sub-model of a comprehensive three-dimensional ice sheet model, the open-source Parallel Ice Sheet Model (PISM; pism-docs.org). To satisfy our goals the new hydrology model must be parallelizable, apply at a wide variety of spatial and temporal scales, exhibit convergence of solutions under grid refinement, and have as few parameters as practical. We will demonstrate that we have succeeded in these goals.

The cavities in our modeled distributed system open by sliding of the ice over bedrock roughness and they close by ice creep, two physical processes which combine to determine the relationship between water amount and pressure. Pressure is thereby determined non-locally over each connected component of the hydrological system. No functional relation between subglacial water amount and pressure is assumed (compare Flowers and Clarke, 2002a). The subglacial 140 water pressure solves an equation which is a parabolic regularization of the distributed pressure equation given in elliptic variational inequality form by Schoof et al. (2012).

In cases where boreholes have actually been drilled to the ice base, till is observed (Hooke et al., 1997; Tulaczyk 145 et al., 2000a; Truffer et al., 2000; Truffer and Harrison, 2006). Laboratory experiments on the rheology of till (Kamb, 1991; Hooke et al., 1997; Tulaczyk et al., 2000a; Truffer et al., 2001) generally conclude that its deformation is well-approximated by a Mohr-Coulomb relation (Schoof, 2006b). For this reason we adopt a compressible-Coulomb-plastic till model when determining the effective pressure on the till as a function of the amount of water stored in the till (Tulaczyk et al., 2000a). Existing models which combine till 150 and a mass conservation equation for the subglacial water are rather different from ours, as they either have only one-horizontal dimension (van der Wel et al., 2013) or have a pressure equation which directly ties water pressure to water amount, which generates a porous medium equation form (Flowers and Clarke, 2002a; de Fleurian et al., 2014). Also 155 unlike ours, these models have not been tested at any scale larger than a single ice stream or glacier.

Wall melt in the linked-cavity system can be calculated diagnostically from the modeled flux and hydraulic gradient. If included as a contribution to the mass conservation equation, however, the addition of wall melt generates an unstable 160 distributed system (Walder, 1982), though such a system can be stabilized to some degree by bedrock bumps (Creyts and Schoof, 2009).

Conduits are not included in our model. While the pressure 165 and amount of water in conduits could evolve by physical processes, the existing theory of conduits apparently requires their locations to be fixed a priori (Schoof, 2010b; Pimentel and Flowers, 2011; Hewitt et al., 2012; Hewitt, 2013; Werder

et al., 2013). Such lattice models have no known continuum limit in the map plane. Because all PISM usage involves a run-time determination of grid resolution, which varies from 40 km to 10 mm in the applications documented in the PISM User’s Manual (PISM authors, 2013), and because all parameters in PISM models must have grid-spacing-independent meaning, such lattice or other fixed-grid models are not acceptable as components of PISM.

The structure of the paper is as follows: Section 2 considers the basic physical principles, culminating with a fundamental advection-diffusion form of the mass conservation equation. Section 3 reviews what is known about till mechanical properties, water in till pore spaces, and shear stress at the base of a glacier. In section 4 we consider cavity evolution, which then leads to a review of closures which determine the subglacial water pressure (section 5). Based on all these elements, in section 6 we state the combined model and its major parameters. In section 7 the simplified equations which apply in steady state are analyzed, and a steady-state functional relationship between water amount and pressure is derived. In section 8 we compute an exact steady solution, a useful tool for verification. In section 9 we present all numerical schemes, with particular attention to time step restrictions and the treatment of advection. Like other parts of PISM, all the numerical schemes are implemented in parallel using the PETSc library (Balay et al., 2011). Section 10 documents the major options and parameters seen by a PISM user. Section 11 shows numerical results from the model, starting with showing convergence under grid refinement in the verification case. Then we demonstrate the model at scale, with five year runs on a 2 km grid covering the entire Greenland ice sheet.

2 Elements of subglacial hydrology

2.1 Mass conservation

We assume that liquid water is of constant density. Thus the thickness of the layer of laterally-transportable (mobile) water, denoted by $W(t, x, y)$, determines its mass. In addition there is liquid water stored locally in the pore spaces of till (Tulaczyk et al., 2000b) which is also described by an effective thickness $W_{\text{til}}(t, x, y)$.

Such thicknesses are only meaningful compared to observations if they are regarded as averages over a horizontal scale of tens to thousands of meters (Flowers and Clarke, 2002a). While the thickness W describes the amount of water in subglacial cavities, and in the connections between cavities (Kamb, 1987), the water in till pore spaces is much less mobile because of the very low hydraulic conductivity of till (Lingle and Brown, 1987; Tulaczyk et al., 2000a; Truffer et al., 2001). Our model includes, however, a model for the strength of the pressurized till (Section 3).

The total effective thickness of the water at map-plane location (x, y) and time t is $W + W_{\text{til}}$. This sum is the conserved quantity in our model. In two map-plane dimensions the mass conservation equation is (compare Clarke, 2005)

$$\frac{\partial W}{\partial t} + \frac{\partial W_{\text{til}}}{\partial t} + \nabla \cdot \mathbf{q} = \frac{m}{\rho_w} \quad (1)$$

where $\nabla \cdot = (\partial/\partial x) + (\partial/\partial y)$, \mathbf{q} is the (vector) water flux (units $\text{m}^2 \text{s}^{-1}$), m is the total input to the subglacial hydrology (units $\text{kg m}^{-2} \text{s}^{-1}$) and ρ_w is the density of fresh liquid water (units kg m^{-3}). The water flux \mathbf{q} is concentrated within a two-dimensional subglacial layer.

The water source m in equation (1) includes melt on the lower surface of the glacier and drainage from the glacier surface if that occurs. In portions of ice sheets with cold surface conditions, such as Antarctica and the interior of Greenland, the basal melt rate part of m is determined by the energy balance at the base of the ice (Aschwanden et al., 2012). The Greenland results in section 11 use only such basal melt as water sources. Drainage from the surface has also been added to m in applications of our model (van Pelt, 2013), but modelling such drainage is outside the scope of this paper.

2.2 Hydraulic potential

The hydraulic potential $\psi(t, x, y)$, which will drive the transport of water, combines the pressure $P(t, x, y)$ of the transportable subglacial water and the gravitational potential of the top of the water layer (Goeller et al., 2013; Hewitt et al., 2012), thus

$$\psi = P + \rho_w g (b + W). \quad (2)$$

Here ρ_w is the water density (kg m^{-3}), g is the acceleration of gravity (m s^{-2}), and $z = b(x, y)$ (m) is the bedrock elevation.

We have added the term “ $\rho_w g W$ ” to the standard hydraulic potential formula $\psi = P + \rho_w g b$ (Clarke, 2005; Shreve, 1972) because differences in the potential at the *top* of the subglacial water layer determine the driving potential gradient for a fluid layer. When W is small then ignoring this term may do no harm. However, when considering local minima of the hydraulic potential, subglacial lakes of finite (not infinitesimal) extent and finite (not infinite) depth should form (compare Le Brocq et al., 2009). The W term in (2) makes the mass conservation equation diffusive, regardless of the action of other diffusive mechanisms; see section 7. When the water depth becomes substantial ($W \gg 1 \text{ m}$), as it would be in a subglacial lake, this term keeps the modeled lakes from being singularities of the water thickness field. Note that only the transportable water W , and not the total water $W + W_{\text{til}}$, is used to determine the potential, again because of the low hydraulic conductivity of till.

Ice in a glacier is a viscous fluid which has a stress field of its own. The basal value of the downward normal stress is traditionally called the *overburden pressure*, which we denote by P_o . We accept the shallow approximation that it is

hydrostatic (Greve and Blatter, 2009):

$$P_o = \rho_i g H, \quad (3)$$

where ρ_i is the density of ice (kg m^{-3}) and H is the ice thickness (m). Because the condition $P > P_o$ is presumed to cause the ice to lift and thus reduce the pressure back to overburden $P = P_o$ (Schoof et al., 2012), it follows that the pressure solution is subject to inequalities

$$0 \leq P \leq P_o. \quad (4)$$

In temperate glaciers an alternative, though approximate, explanation of bounds like (4) can be offered, namely that water rises to the surface through efficient englacial conduits, appearing at the surface and thus ensuring $P \lesssim 1.1 P_o$ (Bartholomäus et al., 2011).

2.3 Darcy flow

The transportable water flows from high to low hydraulic potential. The simplest expression of this is a Darcy flux model for a water sheet,

$$\mathbf{q} = -K W \nabla \psi \quad (5)$$

where K , the hydraulic conductivity, is constant (Clarke, 2005). More generally Schoof et al. (2012) suggests

$$\mathbf{q} = -k W^\alpha |\nabla \psi|^{\beta-2} \nabla \psi \quad (6)$$

for $\alpha \geq 1$, $\beta > 1$, and a coefficient $k > 0$ with units that depend on α and β . Power-law form (6) is justified as an instance of a Manning or Darcy-Weisbach law (Schoof et al., 2012). Clarke (2005) suggests $\alpha = 1$ and $\beta = 2$, to give (5) above, Creyts and Schoof (2009) use $\alpha = 3/2$ and $\beta = 3/2$, Hewitt (2011, 2013) uses $\alpha = 3$ and $\beta = 2$, and Hewitt et al. (2012) suggest $\alpha = 5/4$ and $\beta = 3/2$. The current paper implements law (6) generally but uses the Clarke (2005) and Hewitt et al. (2012) exponents in an exact solution and in numerical experiments, respectively. When we use (6) we call $K = k W^{\alpha-1} |\nabla \psi|^{\beta-2}$ the *effective* hydraulic conductivity, so that equation (5) applies formally throughout.

2.4 Advection-diffusion decomposition

Combining (2) and (6), and separating the term proportional to ∇W , we get the flux expression

$$\mathbf{q} = -k W^\alpha |\nabla \psi|^{\beta-2} \nabla (P + \rho_w g b) - \rho_w g k W^\alpha |\nabla \psi|^{\beta-2} \nabla W. \quad (7)$$

The second term with ∇W acts diffusively in the mass conservation equation (1). On the other hand, because P generally scales with the overburden pressure P_o , the first flux term in (7) will dominate in the common situation $|\nabla H| \gg |\nabla W|$. We will see that in near-steady-state circumstances the part

of the transport velocity which is proportional to ∇P is also actually *diffusive* in the mass conservation equation; this is not obvious but it is explained in section 7. In conditions far from steady state, however, the direction of ∇P is different from the direction ∇W .³¹⁰

We will construct our conservative numerical scheme based on decomposition (7). To simplify the model slightly, the small thickness approximation $W \approx 0$ is made inside the absolute value signs in (7), namely³¹⁵

$$|\nabla \psi| \approx |\nabla(P + \rho_w g b)|. \quad (8)$$

This simplification, which makes no change in the $\beta = 2$ case, lets us define the effective hydraulic conductivity as³²⁰

$$K = kW^{\alpha-1} |\nabla(P + \rho_w g b)|^{\beta-2}. \quad (9)$$

In terms of K we define a velocity field and a diffusivity coefficient:³²⁵

$$\mathbf{V} = -K \nabla(P + \rho_w g b), \quad D = \rho_w g K W. \quad (10)$$

Now (7) is a clean advection-diffusion decomposition,³³⁰

$$\mathbf{q} = \mathbf{V} W - D \nabla W. \quad (11)$$

From equations (1) and (11) we now have an advection-diffusion-production equation for the evolution of the water amount:³³⁵

$$\frac{\partial W}{\partial t} + \frac{\partial W_{\text{til}}}{\partial t} = -\nabla \cdot (\mathbf{V} W) + \nabla \cdot (D \nabla W) + \frac{m}{\rho_w}. \quad (12)$$

There are distinct numerical schemes (section 9) for the advection term $\nabla \cdot (\mathbf{V} W)$ and the diffusion term $\nabla \cdot (D \nabla W)$. These different schemes impose time step restrictions of different magnitudes. We will see that equation (12) is often advection-dominated in the sense that $|\mathbf{V} W| \gg |D \nabla W|$.³⁴⁰ However, we again observe that in near-steady conditions where the velocity \mathbf{V} can be almost proportional to $-\nabla W$ there may be no clean separation of advection and diffusion (section 7). Certainly the numerical schemes for advection and diffusion must be tested in combination, and indeed we measure convergence of the combined numerical schemes in section 11.³⁴⁵

As is well known (Clarke, 2005), the flux \mathbf{q} depends significantly on the ice surface slope because the ice overburden pressure dominates the subglacial water pressure (Shreve, 1972). Therefore the gradient of the hydraulic potential often has the same direction as the ice surface gradient. The model in this paper also generates pressure fields with this property in some circumstances, but the directions of hydraulic potential and surface gradients are significantly different in general because the pressure depends on physical mechanisms for the opening and closing of cavities.³⁵⁰

3 Till hydrology and mechanics

Till with pressurized liquid water in its pore spaces can be expected to support much of the ice overburden. When present, such saturated till is central to the complicated relationship between the amount of subglacial water and the amount of sliding. Our model includes storage of subglacial water in till, potentially everywhere under the ice sheet, both because of its role in conserving the mass of liquid water and its role in determining basal shear stress.

We will assume throughout that liquid water or ice fills pore spaces in the till, and that there are no air- or vapor-filled pore spaces. Recalling that water production under the interior of ice sheets is determined by basal thermodynamics, including geothermal flux and friction-heating, we suppose that when $m = 0$ and $W_{\text{til}} = 0$ then the pore spaces in the till are filled with ice and the basal shear stress is correspondingly-high. When W_{til} but small the till will generally have both liquid water and ice in the pore spaces, and only when W_{til} attains sufficiently large values is the till conceived-of as entirely melted, at which point a drop in effective pressure becomes possible (subsection 3.2 below).

3.1 Evolution of water amount

We choose an evolution equation for W_{til} for simplicity (Bueler and Brown, 2009), namely

$$\frac{\partial W_{\text{til}}}{\partial t} = \frac{m}{\rho_w} - C_d. \quad (13)$$

Here $C_d \geq 0$ is a fixed rate that makes the till gradually drain in the absence of water input. In practice we choose $C_d = 1$ mm/a, which is small compared to typical values of m/ρ_w . Refreeze is also allowed, as a negative value for m . Note that any water removed from the till enters the transport system; it is conserved. Equation (13) is essentially the same as equation (2) in Tulaczyk et al. (2000b). In section 9 we propose a stable numerical scheme for the combination of (1) and (13), and this scheme satisfies discrete conservation of $W + W_{\text{til}}$ and physical bounds for the discretized values of W and W_{til} .

3.2 Effective pressure on the till

There is extensive evidence that deformation of saturated till is well-modeled by a plastic (Coulomb friction) or nearly-plastic rheology (Hooke et al., 1997; Truffer et al., 2000; Tulaczyk et al., 2000a; Schoof, 2006b). The yield stress τ_c of the saturated till satisfies the Mohr-Coulomb relation

$$\tau_c = c_0 + (\tan \varphi) N_{\text{til}} \quad (14)$$

where c_0 is the till cohesion, φ is the till friction angle, and N_{til} is the effective pressure of the overlying ice on the saturated till (Cuffey and Paterson, 2010).¹

¹The effective pressure $N = P_o - P$ used in the next section for modeling cavity closure is distinct from N_{til} . This distinction is

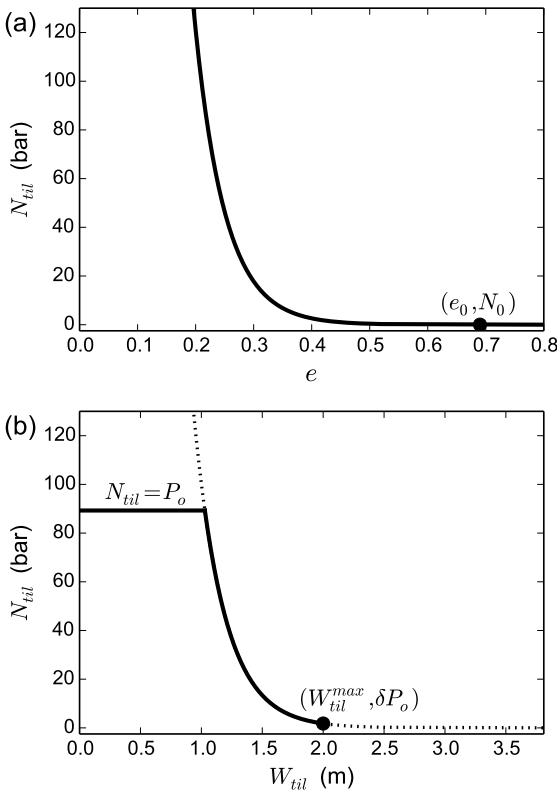


Fig. 1. (a) Equation (16) determines the effective pressure N_{til} as a function of the void ratio e , as shown here. Reference values $e_0 = 0.69$, $N_0 = 10^3$ Pa used by Tulaczyk et al. (2000a) are indicated. (b) In this paper N_{til} is rewritten as a function of W_{til} . It is bounded above by overburden pressure P_o and below by a fixed fraction δ of P_o . Excess water, with $W_{\text{til}} > W_{\text{til}}^{\text{max}}$ and $N_{\text{til}} < \delta P_o$, is “dumped” into the transport system, so we use the bounded model shown as a solid curve, and not the remaining unbounded parts (dotted). The case with 1000 meters ice thickness, $\delta = 0.02$, and $W_{\text{til}}^{\text{max}} = 2.0$ meters is shown.

Let $e = V_w/V_s$ be the till void ratio, where V_w is the volume of water in the pore spaces and V_s is the volume of mineral solids (Tulaczyk et al., 2000a). From the standard theory of soil mechanics and laboratory experiments on till (Hooke et al., 1997; Tulaczyk et al., 2000a), a linear relation exists between the logarithm of N_{til} and e ,

$$e = e_0 - C_c \log_{10}(N_{\text{til}}/N_0). \quad (15)$$

Here e_0 is the void ratio at a reference effective pressure N_0 and C_c is the coefficient of compressibility of the till. Equivalently, N_{til} is an exponential function of e (van der Wel et al., 2013, equation (15)),

$$N_{\text{til}} = N_0 10^{(e_0 - e)/C_c}. \quad (16)$$

justified by the very low hydraulic conductivity of till. Also, N_{til} does not affect the model for the horizontal transport of water.

Figure 1(a) shows a graph of (16). Note that in (15) and (16), N_{til} is nonzero for all finite values of e .

While equations (15) or (16) suggest that the effective pressure could be any positive number, in fact the area-averaged value of N_{til} under ice sheets and glaciers has limits. It cannot exceed the overburden pressure for any sustained period. Furthermore our model of subglacial water movement is that once the till is close to its maximum capacity then the excess water will be “dumped” into a transport system. We suppose this occurs at a small, fixed fraction of the overburden pressure. Thus we assume bounds

$$\delta P_o \leq N_{\text{til}} \leq P_o \quad (17)$$

where $\delta = 0.02$ in the experiments in this paper.

The void ratio e and the effective water layer thickness W_{til} are describing the same thing, namely the amount of liquid water. In fact, if Δx , Δy are the horizontal dimensions of a rectangular patch of till then $V_w = W_{\text{til}} \Delta x \Delta y$ and $V_s = \eta \Delta x \Delta y$ where η is the thickness of the mineral portion of the till. Because $e = V_w/V_s$ it follows that

$$e = \frac{W_{\text{til}}}{\eta}. \quad (18)$$

On the other hand we will describe the maximum capacity of the till by specifying a maximum on the water layer thickness (Bueler and Brown, 2009), that is,

$$0 \leq W_{\text{til}} \leq W_{\text{til}}^{\text{max}}. \quad (19)$$

The minimum $N_{\text{til}} = \delta P_o$ of the effective pressure occurs at the maximum void ratio e , and by (18) W_{til} is also maximum. But then equations (15) and (18) combine to express the solid-till thickness η in terms of our preferred parameters and the overburden pressure,

$$\eta = \frac{W_{\text{til}}^{\text{max}}}{e_0 - C_c \log_{10}(\delta P_o/N_0)}. \quad (20)$$

From (16), (18), and (20), the effective pressure N_{til} can now be written as the following function of W_{til} :

$$N_{\text{til}} = N_0 \left(\frac{\delta P_o}{N_0} \right)^s 10^{(e_0/C_c)(1-s)} \quad (21)$$

where $s = W_{\text{til}}/W_{\text{til}}^{\text{max}}$. However, as noted above, N_{til} is bounded, so the form we use is shown in Figure 1(b):

$$N_{\text{til}} = \min \left\{ P_o, N_0 \left(\frac{\delta P_o}{N_0} \right)^s 10^{(e_0/C_c)(1-s)} \right\}. \quad (22)$$

It follows from equations (14) and (22) that the yield stress τ_c can be determined from the water amount W_{til} . The Mohr-Coulomb relation (14) is, therefore, a relationship $\tau_c(W_{\text{til}})$ in our model. Regarding the parameters in this relation:

- (i) Experiments on till suggest small values for cohesion, $0 \leq c_0 \lesssim 1$ kPa (Tulaczyk et al., 2000a), and we choose $c_0 = 0$ for concreteness.

- (ii) Observed till friction angles φ are in a 18° – 40° range (Cuffey and Paterson, 2010). Simulations of the whole Antarctic (Martin et al., 2011) and Greenlandic (Aschwanden et al., 2013) ice sheets have been based on a hypothesis that the till friction angle φ can depend on bed elevation, so as to accommodate the submarine history of some sediments.
- (iii) The ratio e_0/C_c can be determined by laboratory experiments on till samples (e.g. Hooke et al., 1997; Tulaczyk et al., 2000a). Values for the dimensionless constants e_0 and C_c used in this paper are from till samples from ice stream B in Antarctica, namely $e_0 = 0.69$ and $C_c = 0.12$ in Figure 6 of Tulaczyk et al. (2000a), thus $e_0/C_c = 5.75$.
- (iv) The till capacity parameter W_{til}^{\max} could be set in a location-dependent manner from in situ (Tulaczyk et al., 2000a) or seismic reflection (Rooney et al., 1987) evidence, but for simplicity we set it to a constant 2 meters.

3.3 Sliding law

Ice sliding velocity is determined by solving a stress balance in which the vector basal shear stress τ_b appears either as a boundary condition (Schoof, 2010a) or as a term in the balance (Schoof, 2006a; Bueler and Brown, 2009). In PISM the scalar yield stress τ_c determines the basal shear stress through a sliding law

$$\tau_b = -\tau_c \frac{\mathbf{u}}{|\mathbf{u}|^{1-q} u_0^q} \quad (23)$$

where \mathbf{u} is the sliding velocity of the base of the ice, $0 \leq q \leq 1$, and u_0 is a threshold sliding velocity (Aschwanden et al., 2013). Power law (23) generalizes, and includes as the case $q = 0$, the purely-plastic (Coulomb) relation $\tau_b = -\tau_c \mathbf{u}/|\mathbf{u}|$. At least in the $q \ll 1$ cases, under (23) the till “yields” and the magnitude of the basal shear stress becomes nearly independent of the sliding speed $|\mathbf{u}|$ as it becomes larger than the threshold u_0 . Equation (23) could also be written in generic power-law form $\tau_b = -\beta |\mathbf{u}|^{q-1} \mathbf{u}$ with coefficient $\beta = \tau_c/u_0^q$; this includes the linear case $q = 1$ in which we have $\beta = \tau_c/u_0$.

4 Capacity of a linked-cavity distributed system

The evolution of the area-averaged thickness of the cavities in a distributed linked-cavity system can be described as the difference of opening and closing rates (Hewitt, 2011). This thickness Y , also called the bed separation (Bartholomaeus et al., 2011), has evolution equation

$$\frac{\partial Y}{\partial t} = \mathcal{O}(|\mathbf{v}_b|, Y) - \mathcal{C}(N, Y) \quad (24)$$

where \mathbf{v}_b is the ice base (sliding) velocity and $N = P_o - P$ is the effective pressure on the cavity system. Denoting $X_+ = \max\{0, X\}$, we choose an opening term based on cavitation only:

$$\mathcal{O}(|\mathbf{v}_b|, Y) = c_1 |\mathbf{v}_b| (W_r - Y)_+. \quad (25)$$

Here W_r is a maximum roughness scale of the basal topography (Schoof et al., 2012) and c_1 is a constant. The closing term models ice creep only (Hewitt, 2011; Schoof et al., 2012):

$$\mathcal{C}(N, Y) = c_2 A N^3 Y. \quad (26)$$

Here A is the ice softness and c_2 is a constant which must be constrained by observations. We have used Glen exponent $n = 3$ for concreteness and simplicity.

Equation (24) describes the evolution of the upper surface of the subglacial cavities. By (25) the opening term \mathcal{O} is non-negative. The closing term \mathcal{C} in (26) is also nonnegative because our modeled pressure P satisfies bounds $0 \leq P \leq P_o$. The opening and closing terms (25) and (26) satisfy the inequalities (2.5)–(2.7) in Schoof et al. (2012).

The physical intuition behind a pressure model which combines (24) with mass conservation (1) and a Darcy flux relation like (6) is as follows. If the cavity is larger than local water sources can immediately fill then the pressure should drop. Lower pressure encourages water inflow and, by (26), it speeds cavity closure, bringing the pressure back up. Conversely, if local water sources exceed capacity then increased pressure should push water out of the area, and also creep closure slows. This “intuition” requires a pressure closure, however, which is addressed in the next section.

5 Closures to determine pressure

The evolution equations listed so far, namely (12), (13), and (24), can be simplified to three equations in the four major (state) variables W , W_{til} , Y , and P . We do not yet know how to compute the water pressure P given the other variables and data of the problem. A closure is needed.

5.1 Simplified closures without cavity evolution

We first consider two simple closures which appear in the literature but which do not use cavity evolution equation (24) or similar physics. These simplified closures differ in their physical motivation and the form of their mass conservation equations. We list them because the resulting simplified conservation equations emerge as steady-state reductions of our more complete theory. For simplicity we present them without till storage, that is, with $W_{\text{til}}^{\max} = 0$ in previous equations. We state only the constant conductivity case ($\alpha = 1$ and $\beta = 2$ in equation (6)).

Setting the pressure equal to the overburden pressure is the simplest closure (Le Brocq et al., 2009; Shreve, 1972):

$$P = P_o. \quad (27)$$

This model is sometimes used for “routing” subglacial water under ice sheets so as to identify subglacial lake locations (Livingstone et al., 2013; Siegert et al., 2009). Straightforward calculations using equations (1), (6), and (27) show that the advection-diffusion form (12) has an ice-geometry-determined velocity,

$$\frac{\partial W}{\partial t} = -\nabla \cdot (\tilde{\mathbf{V}} W) + \nabla \cdot (\rho_w g k W \nabla W) + \frac{m}{\rho_w} \quad (28)$$

where

$$\tilde{\mathbf{V}} = -\rho_w g k \left[\frac{\rho_i}{\rho_w} \nabla h + \left(1 - \frac{\rho_i}{\rho_w} \right) \nabla b \right]. \quad (29)$$

Because the approximation $W \ll H$ is usually accepted, so that the hydraulic potential is insensitive to the water layer thickness, i.e. $\psi = P_o + \rho_w g b$ (Le Brocq et al., 2009), the diffusion term $\nabla \cdot (\rho_w g k W \nabla W)$ on the right of (28) is usually not included. With this common simplification, equation (28) becomes a pure advection with a velocity $\tilde{\mathbf{V}}$ which is independent of W . It therefore possesses characteristic curves (Evans, 1998) which are the *a priori* known trajectories of the water flow. These trajectories are determined by ice sheet geometry.

However, without a diffusion term equation (28) exhibits continuum solutions with infinite water concentration at every location where the simplified potential $\psi = P_o + \rho_w g b$ has a minimum, and thus it is not well-posed for evolution of W . In fact, applications using the simplified potential tend to only compute the characteristic curves (i.e. “pathways”, Livingstone et al., 2013) themselves and not the evolving field W . We therefore prefer equation (28) as stated, *with* the diffusion term, because it is well-posed for positive initial and boundary values on W (compare Hewitt et al., 2012). Continuum solutions have finite water layer thickness at all times and solutions will converge under sufficient grid refinement.

At an almost opposite extreme in terms of the mathematical form, the second simplified closure we consider assumes that the water pressure is locally determined by the amount of water. Specifically, Flowers and Clarke (2002a) propose

$$P_{FC}(W) = P_o \left(\frac{W}{W_{crit}} \right)^{7/2}. \quad (30)$$

For Trapridge glacier Flowers and Clarke (2002b) use $W_{crit} = 0.1$ m. Because of the local relation between water amount and pressure, implementation of a coupled ice flow and subglacial hydrology model is simplified because no pressure evolution equation needs to be solved (Pimentel et al., 2010; Pimentel and Flowers, 2011). One obvious concern with form (30) is that $P_{FC}(W)$ can be arbitrarily larger than overburden pressure for large amounts of water (Schoof et al., 2012).

In the flat bedrock case $\nabla b = 0$, we can derive an equation from (1), (6), and (30), namely

$$\frac{\partial W}{\partial t} = \nabla \cdot (k W \nabla P_{FC}(W)) + \frac{m}{\rho_w}. \quad (31)$$

Equation (31) is a nonlinear diffusion which generalizes the porous-medium equation $\partial W / \partial t = \nabla^2(W^\gamma)$ (Schoof et al., 2012; Vázquez, 2007). The main idea in such a nonlinear diffusion is that the direction of the flux is $-\nabla W$. Physically, however, it would seem that $\mathbf{q} \sim -\nabla \psi$ would give flux directions different from $-\nabla W$ in many cases, especially in rapidly-evolving hydrologic systems.

5.2 Full-cavity closure

Requiring the subglacial layer to be full of water is a closure for the subglacial pressure P . We adopt it in our model:

$$W = Y. \quad (32)$$

The consequences of this closure are explored at some length by Schoof et al. (2012), Hewitt et al. (2012), and Werder et al. (2013). They describe the case where cavities are full as the “normal pressure” condition (e.g. equation (4.13) in Schoof et al. (2012)).

Equation (32) obviously allows us to eliminate either W or Y as a state variable. We choose to eliminate Y because W is part of the conserved mass $W + W_{til}$. Using equations (1), (24), and (32) we can derive

$$\mathcal{O}(|\mathbf{v}_b|, W) - \mathcal{C}(N, W) + \frac{\partial W_{til}}{\partial t} + \nabla \cdot \mathbf{q} = \frac{m}{\rho_w}. \quad (33)$$

In the zero till storage case (set $W_{til}^{\max} = 0$ so $W_{til} = 0$), equation (33) is exactly the elliptic pressure equation (2.12) of Schoof et al. (2012). Given values for the water amount W , they solve (33) with pressure boundary conditions at the lateral edges of the subglacial hydrologic system to determine the pressure P .

Schoof et al. (2012) argue that a model based on (33) should accommodate the possibility of partially-empty cavities with $W < Y$ and at zero pressure $P = 0$. As evidence for such vapor/air-filled cavities does not exist for tidewater glaciers or ice sheets, though of course subglacial hydrology is poorly-observed generally, we accept a potential loss of model completeness by using a full-cavity model. An overpressure condition $P > P_o$ has been observed in ice sheets (Das et al., 2008, for example), but only for short durations. Unlike Werder et al. (2013), our modelled pressure satisfies $P \leq P_o$, as would the computationally-expensive elliptic variational inequality model of Schoof et al. (2012).

5.3 Notional englacial porosity as a regularization

Englacial systems of cracks, crevasses, and moulin have been observed in glaciers (Fountain et al., 2005; Bartholomäus et al., 2008; Harper et al., 2010, for example), and these have been included in combined englacial/subglacial hydrology models (Flowers and Clarke, 2002a; Bartholomäus et al., 2011; Hewitt, 2013; Werder et al., 2013). The englacial system is generally parameterized as having macroporosity $0 \leq \phi < 1$. If the englacial system is efficiently-connected to the

subglacial water then the amount of englacial water is equivalent to the subglacial pressure. Thus, in such an englacial hydrologic system, higher or lower subglacial pressure is reflected by higher or lower “water table.”

Bueler (2014) shows that an extension of the lumped englacial/subglacial model in Bartholomäus et al. (2011) to the distributed case gives an equation similar to (33), but with the crucial difference that the equation is parabolic for the pressure and not elliptic (compare Hewitt et al. (2012)). The time-derivative term is proportional to the englacial porosity ϕ . Based on this re-analysis of Bartholomäus et al. (2011), we use this parabolic equation in our model with constant notional englacial porosity $\phi = \phi_0$:

$$\frac{\phi_0}{\rho_w g} \frac{\partial P}{\partial t} = -\nabla \cdot \mathbf{q} + \frac{m}{\rho_w} + \mathcal{C}(N, W) - \mathcal{O}(|\mathbf{v}_b|, W) - \frac{\partial W_{\text{til}}}{\partial t}. \quad (34)$$

Compare equations (7) in Hewitt (2013) and (24) in Werder et al. (2013).

Addition of englacial porosity to the model allows a user-adjustable trade-off between temporal detail in the pressure evolution versus computational effort (van Pelt, 2013). If the englacial porosity ϕ_0 is small, so that there is a nearly impermeable “cap” on the subglacial system, as would occur under a thick ice sheet, then equation (34) is *stiff* and indeed similar, in terms of numerical solution, to an elliptic equation. However, if ϕ_0 is relatively large then equation (34) causes local changes in subglacial pressure P to be damped in the speed and range of their influence on other parts of the connected subglacial hydrologic system.

In fact, equation (34) is stiff to a degree inversely-proportional to ϕ_0 , in the sense that the diffusive range of pressure evolution is proportional to ϕ_0 . The Schoof et al. (2012) theory is the infinitely-stiff $\phi_0 = 0$ case. In general, stiffer equations are harder to solve numerically, and differential-algebraic equations like the system of the mass conservation equation and the elliptic equation (33) are the hardest (Ascher and Petzold, 1998).

Schoof et al. (2012) show that the time-independent mathematical problem encompassing (33) (in the $W_{\text{til}}^{\max} = 0$ case), constraints (4), and appropriate pressure boundary conditions can be written as an elliptic variational inequality (Kinderlehrer and Stampacchia, 1980). This variational inequality problem is asserted to be “numerically prohibitive” by Werder et al. (2013) when solved in two dimensions at each step of a time-stepping model. Instead, in our model we have an explicit time-stepping scheme—see section 9—with adaptive time-stepping to satisfy stability conditions.

Stiffness of pressure equation (34) follows from the incompressibility of water and the relative non-distensibility (i.e. hardness) of the ice and bedrock. Clarke (2003) addresses stiffness in a physically-different but related way by including in his subglacial water equation a relaxation (damping) parameter “ β ” which is based on the small com-

pressibility of water, but which is more than two orders of magnitude larger than the physical value. Clarke’s parameter β appears in his equation exactly as the englacial porosity ϕ_0 appears in equation (34), multiplying the pressure time derivative.

Equation (34) for P is coupled to the advection-diffusion equation (12) for W . Section 9 gives a quantitative analysis of the time-scales related to solving (12) and (34) together.

6 A new subglacial hydrology model in PISM

6.1 Summary of equations and symbols

The major equations for the model are mass conservation (12), Mohr-Coulomb for yield stress (14), till-stored water amount evolution (13), an equation determining till effective pressure from water amount (22), and pressure evolution (34). Recalled here for clarity they are:

$$\begin{aligned} \frac{\partial W}{\partial t} + \frac{\partial W_{\text{til}}}{\partial t} &= -\nabla \cdot (\mathbf{V} W) + \nabla \cdot (D \nabla W) + \frac{m}{\rho_w}, \quad (35) \\ \tau_c &= c_0 + (\tan \varphi) N_{\text{til}}, \\ N_{\text{til}} &= \min \left\{ P_o, N_0 \left(\frac{\delta P_o}{N_0} \right)^s 10^{(e_0/C_c)(1-s)} \right\}, \\ \frac{\partial W_{\text{til}}}{\partial t} &= \frac{m}{\rho_w} - C_d, \\ \frac{\phi_0}{\rho_w g} \frac{\partial P}{\partial t} + \frac{\partial W_{\text{til}}}{\partial t} &= -\nabla \cdot (\mathbf{V} W) + \nabla \cdot (D \nabla W) + \frac{m}{\rho_w} \\ &\quad + c_2 A (P_o - P)^3 W - c_1 |\mathbf{v}_b| (W_r - W)_+. \end{aligned}$$

The above equations use these derived functions:

$D = \rho_w g K W$	diffusivity of W
$K = k W^{\alpha-1} \nabla(P + \rho_w g b) ^{\beta-2}$	effective conductivity
$P_o = \rho_i g H$	overburden pressure
$s = W_{\text{til}} / W_{\text{til}}^{\max}$	W_{til} relative to capacity
$\mathbf{V} = -K \nabla(P + \rho_w g b)$	velocity of W .

The model also includes bounds on the state variables, namely $0 \leq W$, $0 \leq W_{\text{til}} \leq W_{\text{til}}^{\max}$, and $0 \leq P \leq P_o$.

The functions of the model can be categorized into *state* functions, which must be provided with initial values and which evolve according to the model, *data* functions, which are either supplied by observations or by other components of an ice sheet model (e.g. the stress balance in an ice dynamics model will provide $|\mathbf{v}_b|$), and *output* functions which are supplied to other components of the ice sheet model (e.g. the yield stress τ_c is fed back to the stress balance). Thus equations (35) relate the state, data, and output function listed in Table 1, and they require the physical constants and model parameters in Table 2.

The yield stress function τ_c is the most important output of the model. It determines the basal shear stress used in the

Table 1. Functions used in subglacial hydrology model (35).

Type	Description (symbol, units, meaning)
state	W m transportable water thickness
	W_{til} m till-stored water thickness
	P Pa transportable water pressure
data	b m bedrock elevation
	φ till friction angle
	H m ice thickness
	m $\text{kg m}^{-2} \text{s}^{-1}$ total melt water input
output	$ v_b $ ms^{-1} ice sliding speed
	N_{til} Pa till effective pressure
output	τ_c Pa till yield stress

stress balance equations of an ice dynamics model. Full two-way coupling would include the ice dynamics model passing fields b , H , m , and $|v_b|$ to the subglacial hydrology model, and τ_c passed in the other direction.

The model parameters in Table 2 are all constant (i.e. time- and space-independent) in the current paper but they could be allowed to vary spatially if desired. Exploration of the parameter space represented by Table 2 is important, but essentially it is beyond the scope of this model-description paper.

6.2 Reduction to existing models

Four reductions (limiting cases) of model (35) can now be stated precisely:

- (i) The zero till storage ($W_{\text{til}}^{\max} = 0$) and zero englacial porosity ($\phi_0 = 0$) case of (35) is the model described by Schoof et al. (2012), recalling that $\mathbf{q} = -KW\nabla\psi$,

$$\begin{aligned} \frac{\partial W}{\partial t} &= -\nabla \cdot (KW\nabla\psi) + \frac{m}{\rho_w}, \\ 0 &= \nabla \cdot (KW\nabla\psi) + \frac{m}{\rho_w} \\ &\quad + c_2 A(P_o - P)^3 W - c_1 |v_b|(W_r - W)_+. \end{aligned} \quad (36)$$

The bounds $W \geq 0$ and $0 \leq P \leq P_o$ are unchanged. Model (35) is a parabolic regularization of (36) based on a notional connection to porous englacial storage, with a small porosity parameter ϕ_0 , and with coupling to additional till storage; see section 5.

- (ii) The $P = P_o$ limit of (35), in which physical processes for the evolution of pressure are ignored, is the standard model for “routing” water to subglacial lakes under cold ice sheets (Siegert et al., 2009; Livingstone et al., 2013). Assuming again that till storage is removed ($W_{\text{til}}^{\max} = 0$) then the model has only W as a state variable.

The single evolution equation of this reduced model is

$$\frac{\partial W}{\partial t} = -\nabla \cdot (\mathbf{V}W) + \nabla \cdot (D\nabla W) + \frac{m}{\rho_w}. \quad (37)$$

along with the bound $W \geq 0$ and definitions $K = kW^{\alpha-1} |\nabla(P_o + \rho_w gb)|^{\beta-2}$ and $\mathbf{V} = -K\nabla(P_o + \rho_w gb)$. As noted in section 5, the $\alpha = 1$ case of this model routes water with a velocity which is determined entirely by ice and bedrock geometry. Thus this reduced model is essentially an advection, but, because of (2) for the hydraulic potential, which implies some diffusion, model (37) is well-posed and has continuous solutions. Equation (37) therefore represents a modest improvement to the existing “routing” models.

(iii) The non-distributed “lumped” form of (35), in which, in particular, $\nabla \cdot \mathbf{q} = (q_{\text{out}} - q_{\text{in}})/L$ where L is the length of the glacier and $q_{\text{out}}, q_{\text{in}}$ are given by observations, is the porous glacier model of Bartholomäus et al. (2011). The correspondence is further explained in Bueler (2014), with an emphasis on the pressure equation which applies in that lumped model.

(iv) The undrained plastic bed (UPB) model of Tulaczyk et al. (2000b) arises as the $W = 0, \mathbf{q} = 0, \phi_0 = 0$ reduction of (35):

$$\begin{aligned} \frac{\partial W_{\text{til}}}{\partial t} &= \frac{m}{\rho_w} - C_d, \\ \tau_c &= c_0 + (\tan \varphi) N_{\text{til}}, \\ N_{\text{til}} &= N_0 10^{(e_0 - e)/C_c}, \end{aligned} \quad (38)$$

along with equations (18) and (20) relating void ratio e to the thickness W_{til} .

This UPB model depends on friction-heating feedback to keep W_{til} bounded, which is not effective in a membrane-stress-inclusive theory in which local friction heating is a non-local function of changes in till strength. Bueler and Brown (2009) therefore enforce $W_{\text{til}} \leq W_{\text{til}}^{\max}$ by non-conservatively removing water above the capacity, which is a minimal “drained” version of the UPB model.

The above list does not imply that all possible subglacial hydrology models are subsumed in ours. For example, the subglacial hydrology model of Johnson and Fastook (2002) could be considered as a variation on idea (ii) above but it cannot be considered a reduction of our model. The Flowers and Clarke (2002a) model is also not a reduction, although a significant connection is explained in the next section on steady states.

Most significantly, models which include conduits (Schoof, 2010b; Pimentel and Flowers, 2011; Hewitt et al., 2012, among others) are not reductions of our model. Conduit evolution is numerically-straightforward to implement in one-dimensional hydrology models (Pimentel and Flowers, 2011; Hewitt et al., 2012; van der Wel et al., 2013) but when extended to two-horizontal dimensions all existing

Table 2. Physical constants and model parameters. Default values are overridden in some experiments.

Name	Default Value	Units	Description
A	3.1689×10^{-24}	$\text{Pa}^{-3} \text{s}^{-1}$	ice softness (Huybrechts et al., 1996)
α	5/4		power in flux formula (Schoof et al., 2012)
β	3/2		power in flux formula (Schoof et al., 2012)
c_0	0	Pa	till cohesion (Tulaczyk et al., 2000a)
c_1	0.5	m^{-1}	cavitation coefficient (Schoof et al., 2012)
c_2	0.04		creep closure coefficient
C_c	0.12		till compressibility (Tulaczyk et al., 2000a)
C_d	0.001	m a^{-1}	background till drainage rate
δ	0.02		N_{til} lower bound, as fraction of overburden pressure
e_0	0.69		reference void ratio at N_0 (Tulaczyk et al., 2000a)
ϕ_0	0.01		notional (regularizing) englacial porosity
g	9.81	m s^{-2}	acceleration of gravity
k	0.001	$\text{m}^{2\beta-\alpha} \text{s}^{2\beta-3} \text{kg}^{1-\beta}$	conductivity coefficient (Schoof et al., 2012)
N_0	1000	Pa	reference effective pressure (Tulaczyk et al., 2000a)
ρ_i	910	kg m^{-3}	ice density (Greve and Blatter, 2009)
ρ_w	1000	kg m^{-3}	fresh water density (Greve and Blatter, 2009)
W_r	0.1	m	roughness scale (Hewitt et al., 2012)
W_{til}^{\max}	2	m	maximum water in till (Bueler and Brown, 2009)

models (Schoof, 2010b; Hewitt, 2013; Werder et al., 2013) become “lattice” models without a known continuum limit.

7 Analysis of steady states

7.1 Equations of steady state

The steady states of equations (35) are of physical modelling importance because the subglacial system can be close to steady state much of the time. In steady state several physical processes become decoupled. In fact we can make four specific observations which are special to steady state, and which we find are useful in understanding the time-dependent model:

- (i) there is a functional relationship $P = P(W)$ which determines the pressure given the water amount,
- (ii) the apparently advective flux “ $\mathbf{V}W$ ” actually acts diffusively if sliding is occurring and the water amount is either small or is comparable to the roughness scale,
- (iii) the water amount generally scales inversely with the conductivity ($W \sim 1/k$), and
- (iv) exact solutions can be constructed.

In this section we address (i), (ii), and (iii), while (iv) is addressed in section 8.

We simplify the model slightly before addressing steady states: fix $\alpha = 1$ and $\beta = 2$, and remove till storage by setting $W_{\text{til}}^{\max} = 0$. The general observations above will apply without these simplifications, but the formulas here are more manageable because of them.

The steady form of model (35), with these simplifications, can be written as follows in terms of $\mathbf{V}, \mathbf{q}, W, P$:

$$\mathbf{V} = -k\nabla(P + \rho_w g b), \quad (39)$$

$$\mathbf{q} = \mathbf{V}W - \rho_w g k W \nabla W, \quad (40)$$

$$0 = -\nabla \cdot \mathbf{q} + \frac{m}{\rho_w}, \quad (41)$$

$$0 = c_2 A (P_o - P)^3 W - c_1 |\mathbf{v}_b| (W_r - W)_+. \quad (42)$$

Note that we also have bounds $W \geq 0$ and $0 \leq P \leq P_o$.

Steady state equations (39)–(42) are stated in the one-dimensional case by Schoof et al. (2012) model, where the decoupling is also noted; see equations (5.8) and (5.10) in (Schoof et al., 2012).

7.2 Pressure as a function of W in steady state

Relative to the time-dependent form (35), we see there are separate balances between the divergence of the flux and the water input on the one hand (equation (41)), and the opening and closing processes on the other hand (equation (42)). The latter balance allows us to write the pressure $P = P(W)$ in steady state as a continuous function of the water amount W .

Steady state is only possible if a condition holds:

$$c_1 |\mathbf{v}_b| (W_r - W)_+ \leq c_2 A P_o^3 W. \quad (43)$$

The reason for this constraint combines the cavity evolution equation (24), in the steady state case, and the full-cavity closure (32), giving (42). But (42) is only possible if the maximum closing rate $\mathcal{C}(N, W)$, which depends on pressure P , can match the opening rate $\mathcal{O}(|\mathbf{v}_b|, W)$, which is pressure-independent. The maximum closure rate occurs at zero water pressure, thus (43).

We define the following scaled basal sliding speed which has units of pressure:

$$s_b = \left(\frac{c_1 |\mathbf{v}_b|}{c_2 A} \right)^{1/3}. \quad (44)$$

One regard s_b as a scale for the pressure drop from cavitation. Then (43) is equivalent to

$$W \geq W_c := \frac{s_b^3}{s_b^3 + P_o^3} W_r. \quad (45)$$

If (43) or (45) holds then

$$P(W) = P_o - s_b \left(\frac{(W_r - W)_+}{W} \right)^{1/3}. \quad (46)$$

Note that in (46) we have $P(W_c) = 0$. Underpressure ($P = 0$) with subcritical water amount ($W < W_c$) does not occur in steady state though it can occur in nonsteady conditions. Formula (46) may apply even if $W \geq W_r$, in which case the water pressure takes the overburden value $P = P_o$.

Figure 2 shows the function $P(W)$ from (46) for different values of sliding speed $|\mathbf{v}_b|$, and Figure 3 for values of overburden pressure P_o . We see that as the water amount reaches the roughness scale ($W \nearrow W_r$) the pressure rises rapidly to overburden ($P(W) \nearrow P_o$). At the other extreme, we see that $P(W) \searrow 0$ as $W \searrow W_c$. The curves $P(W)$ in Figures 2 and 3 do not include the underpressure cases $0 \leq W < W_c$.

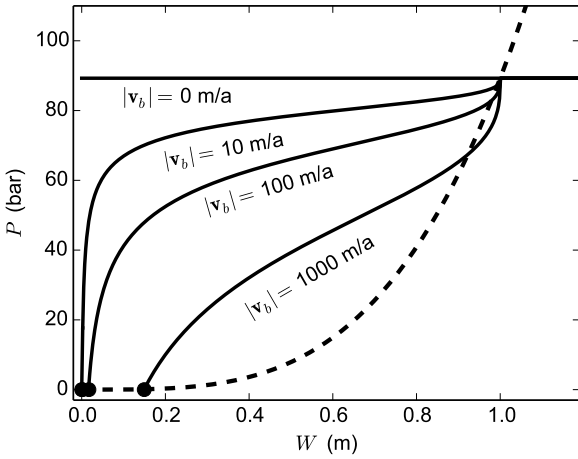


Fig. 2. The steady state function $P(W)$ defined by equation (46) depends on the sliding speed $|\mathbf{v}_b|$. Four cases are shown. All use $W_r = 1$ m and a uniform ice thickness of $H = 1000$ m. Values of W_c are indicated by black dots at $P = 0$. Relation (30) (dashed black) is shown with $W_{\text{crit}} = 1$ m for comparison.

Recall that Flowers and Clarke (2002a) propose function $P_{FC}(W)$ for both steady and nonsteady circumstances. Both functions $P(W)$ in (46) and $P_{FC}(W)$ in (30) are increasing. They both relate the water pressure to the overburden pressure P_o . However, while in (46) the relation to P_o is additive, in (30) it is a multiplicative scaling. The power law

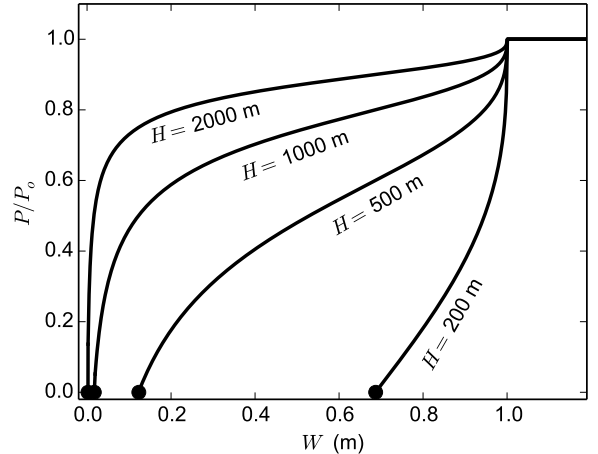


Fig. 3. The graph of $P(W)$ defined by (46) also depends on overburden pressure $P_o = \rho_i g H$. We fix $|\mathbf{v}_b| = 100$ m/a and $W_r = 1$ m and consider four cases of uniform thickness H .

form (30) is not justified by the physical reasoning which led to equation (46), even in steady state. It would appear that any functional relationship $P(W)$ should also depend on the sliding velocity, as it does here, if cavitation influences the water pressure. Of course the $W > W_{\text{crit}}$ case gives $P_{FC}(W) > P_o$ in (30), but this condition does not arise in (46). In conclusion, an important contrast between the Flowers and Clarke (2002a) theory and the current paper is that we will not assume a relationship $P = P(W)$ in nonsteady conditions, even though such a relation emerges in our theory in the steady state case.

7.3 Flux in steady state

We now consider how the steady state water velocity \mathbf{V} , and the associated flux \mathbf{q} , depends on other quantities. Because \mathbf{V} depends on ∇P , according to equations (39) and (46) in steady state we have

$$\frac{\partial P}{\partial W} = \frac{s_b W_r}{3W^{4/3}(W_r - W)^{2/3}} \quad (47)$$

if $W_c < W < W_r$. If $W \leq W_c$ then $\partial P / \partial W$ is undefined, and if $W > W_r$ then $\partial P / \partial W = 0$. Note that the condition $W_c < W < W_r$ corresponds to the pressure condition $0 < P < P_o$ in steady state. Formula (47) and Figures 2 and 3 agree that $\partial P / \partial W \rightarrow \infty$ as $W \nearrow W_r$. Equations (39), (46), and (47) imply a formula for the velocity in steady state:

$$\mathbf{V} = -k \left[\nabla \psi_o - \left(\frac{W_r - W}{W} \right)^{1/3} \nabla s_b + \frac{s_b W_r}{3W^{4/3}(W_r - W)^{2/3}} \nabla W \right], \quad (48)$$

where $\psi_o = P_o + \rho_w g b$.

Formula (48) helps us understand the steady state meaning of the advective flux “ $\mathbf{V}\mathbf{W}$ ” in $\mathbf{q} = \mathbf{V}\mathbf{W} - D\nabla W$. The direc-

tion of water velocity \mathbf{V} is determined by a combination of a geometric direction ($\nabla\psi_o$), a direction derived from spatial variations in the sliding speed (∇s_b), and a diffusive direction (∇W). Thus a portion of $\mathbf{V}W$ is diffusive in steady state, in addition to the *a priori* diffusive flux $-D\nabla W$. In fact we can write the flux as a linear combination of gradients,

$$\mathbf{q} = -kA_1\nabla\psi_o + kA_2\nabla s_b - kA_3\nabla W, \quad (49)$$

with coefficients

$$A_1 = W, \quad (50)$$

$$A_2 = (W_r - W)^{1/3}W^{2/3},$$

$$A_3 = \frac{s_b W_r}{3(W_r - W)^{2/3}W^{1/3}} + \rho_w g W.$$

The first two coefficients A_1, A_2 go to zero as $W \rightarrow 0$, but A_3 remains large when $W \rightarrow 0$ as long as sliding is occurring ($s_b > 0$). Thus for low water amount and sustained sliding we should think of the water as diffusing in the layer. When the water thickness is greater, namely if it is almost the roughness scale ($W \lesssim W_r$), then A_3 is large in sliding cases ($s_b > 0$); again the effect is diffusive.

Thinking more generally, it is not surprising that when the ice thickness, bed elevation, sliding velocity, or water thickness fields are highly-variable in space then we can expect larger speeds $|\mathbf{V}|$ in steady state. The various gradients in formula (49) reflect this general intuition. Because the magnitude of the velocity determines the CFL time step restriction (Morton and Mayers, 2005), large variations in these spatial fields will generally shorten time steps; see section 9.

7.4 Hydraulic conductivity in steady state

Our next observation takes advantage of the above analysis of the flux in steady state: the water amount W roughly scales with $1/k$ where k is the hydraulic conductivity. In fact, if we combine equation (41) with (49) and rearrange slightly then we find

$$-\nabla \cdot (A_3 \nabla W) = \frac{m}{k\rho_w} + \nabla \cdot (A_1 \nabla \psi_o) - \nabla \cdot (A_2 \nabla s_b). \quad (51)$$

One may regard (51) as a non-linear elliptic equation for W . In fact, in the case where H , b , and $|\mathbf{v}_b|$ are all spatially-uniform, so that $\nabla\psi_o = \nabla s_b = 0$, equation (51) is of the form $-\nabla \cdot (A_3(W) \nabla W) = m/(k\rho_w)$ where $A_3(W) = A_3$ is given in (50). If W is both bounded away from zero and bounded away from the roughness scale W_r (i.e. there is $\epsilon > 0$ so that $\epsilon < W < W_r - \epsilon$) then this equation is uniformly elliptic. Thus a maximum principle applies (Evans, 1998). This means that if there is a nonnegative basal melt rate in any region then the maximum of W will equal or exceed the maximum of W along the boundary of that region, so the graph of W is concave down. However, if $W \approx 0$ or $W \lesssim W_r$ then the diffusivity coefficient $A_3(W)$ will be

large and so the values of W away from the boundary will be flattened-out by the resulting fast diffusion.

Furthermore the values of W will scale with $1/k$. Indeed, for the simpler equation $-\nabla \cdot (D_0 \nabla W) = m_0/(k\rho_w)$, with D_0, m_0 positive constants, on a disc of radius L , and zero boundary values, the solution $W(r) = m_0(1 - (r/L)^2)/(4kD_0\rho_w)$ has a maximum value $W(0)$ which precisely scales as $1/k$. As seen in numerical results, the solution W of (51) will also scale with $1/k$ if $\nabla\psi_o$ and ∇s_b are not too large, though fast-diffusion flattening of the maximum of W will occur when W is close to the limits of the interval $[0, W_r]$.

8 An exact steady state solution

8.1 Radial equations

The above steady equations are the basis on which we now build a nearly-exact solution for W and P in the map-plane, in a case with nontrivial overburden pressure and nontrivial ice sliding speed. This solution, which is useful for verifying numerical schemes, depends on the numerical solution of a scalar first-order ordinary differential equation (ODE) initial value problem, something we can do with high accuracy. Traveling wave exact solutions in one horizontal dimension appear in Schoof et al. (2012).

Consider steady state equations (39)–(41), and assume all quantities only depend on the radial coordinate $r = \sqrt{x^2 + y^2}$. One may eliminate \mathbf{V} . In the flat bed case ($b = 0$) the resulting pair of equations is

$$q = -kW \left(\frac{dP}{dr} + \rho_w g \frac{dW}{dr} \right), \quad (52)$$

$$\frac{1}{r} \frac{d}{dr} (rq) = \frac{m}{\rho_w}. \quad (53)$$

In the case of constant water input where $m = m_0 > 0$, which we assume for the exact solution, we can integrate (53) from 0 to r and use symmetry ($q(0) = 0$) to get

$$q(r) = \frac{m_0}{2\rho_w} r. \quad (54)$$

Suppose $h(r)$ is given so that $P_o(r)$ is also determined. Assume that the scaled sliding speed $s_b(r)$ has a bounded derivative and that the solution $W(r)$ satisfies conditions $W_c < W < W_r$; these properties can be verified for the constructed solution. By combining (46), (47), (52), and (54) we can eliminate q and P to find

$$\begin{aligned} \omega_0 r = -W \left[\frac{dP_o}{dr} - \frac{ds_b}{dr} \left(\frac{W_r - W}{W} \right)^{1/3} \right. \\ \left. + \left(\frac{s_b W_r}{3W^{4/3}(W_r - W)^{2/3}} + \rho_w g \right) \frac{dW}{dr} \right] \end{aligned} \quad (55)$$

where $\omega_0 = m_0/(2\rho_w k)$.

Equation (55) is a first-order ordinary differential equation (ODE) for $W(r)$. To put it in the standard form expected by a numerical ODE solver we solve it for dW/dr :

$$\frac{dW}{dr} = \frac{\frac{ds_b}{dr} W \tilde{W} - \left[\omega_0 r W^{-1} + \frac{dP_o}{dr} \right] W^{4/3} \tilde{W}^{2/3}}{\frac{1}{3} s_b W_r + \rho_w g W^{4/3} \tilde{W}^{2/3}}. \quad (56)$$

where $\tilde{W} = W_r - W$ is the amount by which the water is below the roughness scale.

8.2 A nontrivial solution

Though equation (56) has a constant solution $W(r) = W_r$, to generate a nontrivial exact solution we will choose a positive thickness of ice at the margin (a cliff) so that $P_o(L^-) > 0$. At the ice margin $r = L$ we have water pressure $P = 0$ so $W(L) = W_c(L^-)$ is the boundary condition for the ODE. We assume that at the margin there is some sliding so that $s_b(L^-) > 0$, and by (43) we require that $s_b(L^-)W_r > P_o(L^-)^3 W(L)$. The condition at $r = L$ also satisfies $W(L) < W_r$. Then we integrate (56) from $r = L$ to $r = 0$. The central water thickness value $W(0)$ is determined as part of the solution.

It is useful to have an ice cap geometry in which the surface gradient formula is simple so that dP_o/dr in (56) is also simple, so we choose a parabolic profile

$$H(r) = H_0 \left(1 - \frac{r^2}{R_0^2} \right) \quad (57)$$

where $H(0) = H_0$ is the height of the center of the ice cap. It follows that $dP_o/dr = -Cr$ where $C = 2\rho_i g h_0 R_0^{-2}$. We choose $L = 0.9R_0$ and we note that $H(L) = 0.19h_0$ is the size of the cliff.

The sliding speed could be determined by a model for stresses at the ice base and within the ice (Greve and Blatter, 2009), but a coupled ice and water dynamics solution is unnecessary for hydrology model verification. Instead we choose a well-behaved sliding speed function which has no sliding near the ice cap center, until a radius $r = R_1$ at which sliding starts and then increases in the radial direction:

$$|\mathbf{v}_b|(r) = \begin{cases} 0, & 0 \leq r \leq R_1, \\ v_0 \left(\frac{r-R_1}{L-R_1} \right)^5, & R_1 < r \leq L. \end{cases} \quad (58)$$

It follows from (44) and (58) that ds_b/dr in (56) is bounded and continuous on $0 \leq r \leq L$.

Now we solve ODE (56) with initial condition $W(L)$ and using the specific values in Table 3. We use adaptive numerical ODE solvers, both a Runge-Kutta 4(5) Dormand-Prince method and a variable-order stiff solver, with relative tolerance 10^{-12} and absolute tolerance 10^{-9} . The two solvers gave essentially identical results. Modest stiffness (Ascher and Petzold, 1998) of ODE (56) is observed at $r \approx R_1$. The result $W(r)$ is shown in Figure 4.

Because equations (57) and (58) imply a pressure functional relation $P = P(W, r)$ from (46), we can also show in Figure 4 the regions of the r, W plane which correspond to overpressure, normal pressure, and underpressure. We see that $W(r)$ is in the normal pressure region as r decreases from $r = L$ to $r = R_1$, but at $r = R_1$ the function $W(r)$ switches into the overpressure case because there is no sliding. Figure 5 shows the corresponding pressure solution $P(r) = P(W(r))$ from (46).

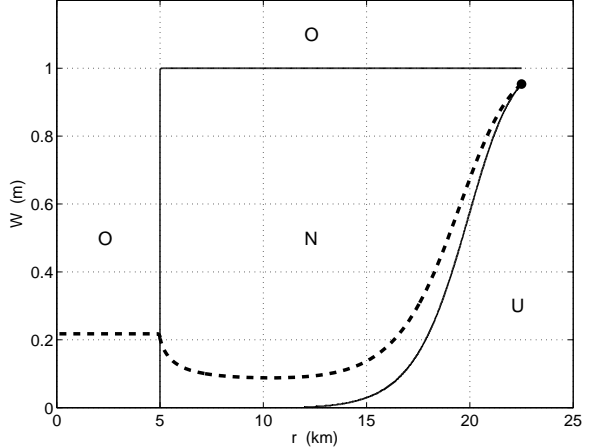


Fig. 4. An exact radial, steady solution for water thickness $W(r)$ (dashed). In r -versus- W space the overpressure (O), normal pressure (N), and underpressure (U) regions are determined by ice geometry and sliding velocity (solid curves; see text).

The reason for stiffness near R_1 is that as the sliding goes to zero the cavitation rate goes to zero. Because creep closure balances cavitation in steady state, effective pressure also goes to zero ($P \rightarrow P_o$). The remaining active mechanisms in the model are the variable overburden pressure and the rate of water input, and they must exactly balance. In this case (56) reduces to the simpler form

$$\frac{dW}{dr} = -\frac{\varphi_o r W^{-1} + \frac{dP_o}{dr}}{\rho_w g}. \quad (59)$$

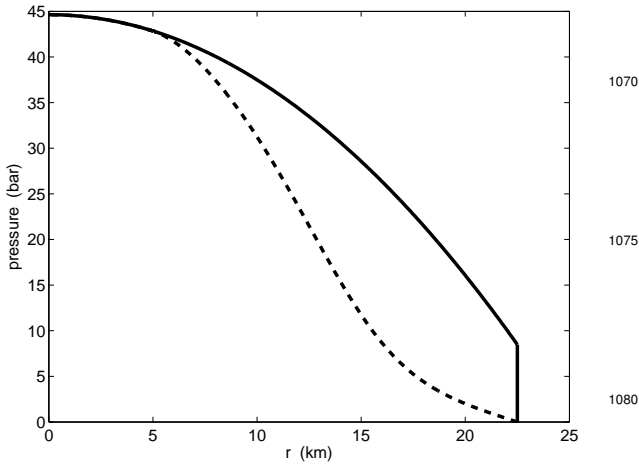
Though we have not derived it this way, Equation (59) is the steady radial form of the mass conservation equation under the “ $P = P_o$ ” closure, namely equation (28).

In equation (59) we see that $dW/dr = 0$ if W satisfies $W = -\omega_0 r / (dP_o/dr)$. In our case with geometry (57) this reduces to a constant value $W = W^* = 0.21764$ m because dP_o/dr is linear in r . Both numerical ODE solvers used here confirm that $W(r)$ is asymptotic to this constant value W^* as $r \rightarrow 0$, and that $W(r) \approx W^*$ within about 1% on all of $0 \leq r \leq R_1$. This is seen in Figure 4.

In summary, we have derived and analyzed an exact solution, in a case with angular symmetry, of the steady state form of the coupled model (35), assuming $W_{\text{til}}^{\max} = 0$ and $b = 0$. This solution will be helpful in verifying the numerical schemes in the next section.

Table 3. Constants used in constructing the exact solution.

Name	Value	Units	Description
α	1		power in flux
β	2		power in flux
H_0	500	m	ice cap center thickness
k	$0.01/(\rho_w g)$	$\text{m}^3 \text{s kg}^{-1}$	hydraulic conductivity
L	22.5	km	$= 0.9R_0$; location of cliff
m_0	$0.2\rho_w$	$\text{kg m}^{-2} \text{a}^{-1}$	constant water input rate; $= 20 \text{ cm a}^{-1}$
R_0	25	km	ideal ice cap radius (at which $H \rightarrow 0$)
R_1	5	km	radial location $r = R_1$ of onset of sliding
v_0	100	m a^{-1}	sliding speed scale
W_r	1	m	roughness scale

**Fig. 5.** An exact radial, steady solution pressure $P(r)$ (dashed) and overburden pressure P_o (solid).

The condition $\Delta t \leq \min\{\Delta t_{\text{CFL}}, \Delta t_W\}$ is sufficient for stability and convergence of the scheme for (12). Below we show this for the first-order upwind scheme, but standard theory suggests the same conclusion for the higher-order flux-limited advection scheme (Hundsdorfer and Verwer, 2010).

We can understand the scale of these restrictions better by considering an example using the parameter values in Table 2. We ran the model on a $\Delta x = \Delta y = 250$ m grid to approximate steady state for the subglacial hydrology of Norgenskiöldbreen (van Pelt, 2013; van Pelt et al., 2012), using observed ice and bedrock geometry, a hypothesized water input distribution with average value about 1 m a^{-1} , and a glacier-wide constant sliding rate of 50 m a^{-1} . The result is that the maximum computed water speed $|\mathbf{V}|$ is about 0.2 m s^{-1} so the advective restriction (60) is $\Delta t_{\text{CFL}} \approx 300 \text{ s} \approx 10^{-5} \text{ a}$. Computed diffusivity $D = \rho_w g K W$ has a maximum value that varies significantly in time, $0.1 \leq \max D \leq 5 \text{ m}^2 \text{s}^{-1}$. Diffusive restriction (61) using value $\max D = 1 \text{ m}^2 \text{s}^{-1}$ is $\Delta t_W \approx 8000 \text{ s} \approx 2.5 \times 10^{-4} \text{ a}$. Thus in this simulation $\Delta t_W \approx 25 \Delta t_{\text{CFL}}$.

This example suggests that, unless both the global peak velocity is unusually slow, and deep subglacial lakes develop so that D is large, the diffusive time scale is significantly longer than the CFL time scale for a 250 m grid. The scaling $\Delta t_W = O(\Delta x^2)$ versus $\Delta t_{\text{CFL}} = O(\Delta x^1)$ makes it clear that under sufficient spatial grid refinement Δt_W is the controlling restriction, but we suppose that Δt_{CFL} is controlling for $\Delta x \gg 100$ m. We will see below, however, that the time step restriction associated to an explicit time-stepping method for the pressure equation is typically shorter than either of $\Delta t_W, \Delta t_{\text{CFL}}$, and it scales as $O(\Delta x^2)$ like Δt_W . If implicit time-stepping is used for the pressure equation, which requires variational inequality treatment (Schoof et al., 2012), then the time scales $\Delta t_W, \Delta t_{\text{CFL}}$ addressed here are the only restrictions. The time step restriction Δt_W could be removed by implicit steps for the mass-conservation equation, though it would seem this requires another variational inequality formulation because of the lower bound $W \geq 0$. Our observation that $\Delta t_{\text{CFL}} \ll \Delta t_W$ for practical ice sheet grids suggests that implicit time-stepping for the mass-conservation equation is not beneficial.

9 Numerical schemes

9.1 Mass conservation: time-stepping

Mass conservation equation (12), which is part of the combined mathematical model (35), will be discretized by an explicit, conservative finite difference method. A centered, second-order scheme will be applied to the diffusion part. A pair of schemes for the advection part will be compared, namely first-order upwinding and a higher-order flux-limited upwind-biased method.

We first consider stable time steps. Stability for the advection schemes occurs with a time step $\Delta t \leq \Delta t_{\text{CFL}}$ where

$$\Delta t_{\text{CFL}} \left(\frac{\max|u|}{\Delta x} + \frac{\max|v|}{\Delta y} \right) = \frac{1}{2}. \quad (60)$$

Because of the additional diffusion process, for stability the time step should also satisfy $\Delta t \leq \Delta t_W$ where (Morton and Mayers, 2005)

$$\Delta t_W 2 \max D \left(\frac{1}{\Delta x^2} + \frac{1}{\Delta y^2} \right) = \frac{1}{2}. \quad (61)$$

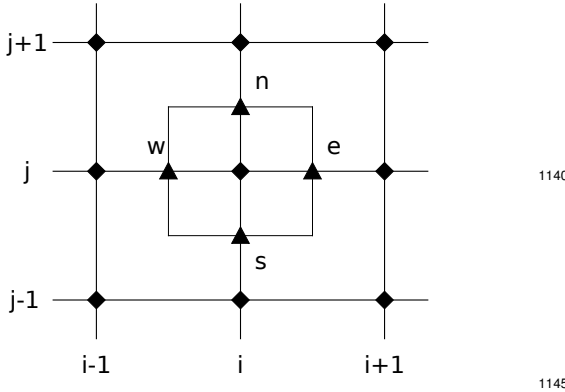


Fig. 6. Numerical schemes (67) and (75) use a grid-point-centered cell. Velocities, diffusivities, and fluxes are evaluated at staggered grid locations (triangles at centers of cell edges denoted e, w, n, s). State functions W, P are located at regular grid points (diamonds). 1150

9.2 Mass conservation: spatial discretization

To set notation, suppose the rectangular computational domain has $M_x \times M_y$ gridpoints (x_i, y_j) with uniform spacing 1155 $\Delta x, \Delta y$. Let $W_{i,j}^l \approx W(t_l, x_i, y_j)$, $(W_{\text{til}})_{i,j}^l \approx W_{\text{til}}(t_l, x_i, y_j)$, and $P_{i,j}^l \approx P(t_l, x_i, y_j)$ denote the numerical approximations. 1160

We will compute velocity components and flux components at the staggered (cell-face-centered) points shown in Figure 6 using centered finite difference approximations of equations (10) and (11). We use “compass” indices such as $u_e = u_{i+1/2,j}$ for the “east” staggered value of u and 1165 $v_n = v_{i,j+1/2}$ for the “north” staggered value of v . Similarly we use compass indices for staggered grid values of the water layer thickness, computed by averaging regular grid values:

$$W_e = (W_{i,j}^l + W_{i+1,j}^l)/2, \quad (62) \quad \text{1165}$$

$$W_n = (W_{i,j}^l + W_{i,j+1}^l)/2.$$

The nonlinear effective conductivity K from (9) is also needed at staggered locations. As a notational convenience define $R = P + \rho_w g b$ and define these staggered-grid values (compare Mahaffy, 1976): 1170

$$\begin{aligned} \Pi_e &= \left| \frac{R_{i+1,j} - R_{i,j}}{\Delta x} \right|^2 \\ &\quad + \left| \frac{R_{i+1,j+1} + R_{i,j+1} - R_{i+1,j-1} - R_{i,j-1}}{4\Delta y} \right|^2, \\ \Pi_n &= \left| \frac{R_{i+1,j+1} + R_{i+1,j} - R_{i-1,j+1} - R_{i-1,j}}{4\Delta x} \right|^2 \\ &\quad + \left| \frac{R_{i,j+1} - R_{i,j}}{\Delta y} \right|^2. \end{aligned}$$

Thereby define 1175

$$K_e = k W_e^{\alpha-1} \Pi_e^{(\beta-2)/2}, \quad K_n = k W_n^{\alpha-1} \Pi_n^{(\beta-2)/2}. \quad (63) \quad \text{1180}$$

The velocity components are then found by differencing:

$$u_e = -K_e \left(\frac{P_{i+1,j} - P_{i,j}}{\Delta x} + \rho_w g \frac{b_{i+1,j} - b_{i,j}}{\Delta x} \right), \quad (64)$$

$$v_n = -K_n \left(\frac{P_{i,j+1} - P_{i,j}}{\Delta y} + \rho_w g \frac{b_{i,j+1} - b_{i,j}}{\Delta y} \right).$$

Similarly for diffusivity we have

$$D_e = \rho_w g K_e W_e, \quad D_n = \rho_w g K_n W_n. \quad (65)$$

We get the remaining staggered-grid quantities by shifting indices:

$$u_w = u_e|_{(i-1,j)}, \quad K_w = K_e|_{(i-1,j)}, \quad D_w = D_e|_{(i-1,j)},$$

$$v_s = v_n|_{(i,j-1)}, \quad K_s = K_n|_{(i,j-1)}, \quad D_s = D_n|_{(i,j-1)}.$$

Now we define $Q_e(u_e)$, $Q_w(u_w)$, $Q_n(v_n)$, and $Q_s(v_s)$ as the face-centered (staggered-grid) normal components of the advective flux $\mathbf{V}W$. These quantities are described in more detail in the next subsection. They use only the staggered velocity component but there is upwinding to determine which W value, or combination of W values, is used.

The grid values of $\nabla \cdot \mathbf{q} = \nabla \cdot (\mathbf{V}W) - \nabla \cdot (D \nabla W)$ using (64) and (65) now become:

$$\begin{aligned} \mathcal{D}_{i,j} &= \frac{Q_e(u_e) - Q_w(u_w)}{\Delta x} + \frac{Q_n(v_n) - Q_s(v_s)}{\Delta y} \quad (66) \\ &\quad - \frac{D_e(W_{i+1,j}^l - W_{i,j}^l) - D_w(W_{i,j}^l - W_{i-1,j}^l)}{\Delta x^2} \\ &\quad - \frac{D_n(W_{i,j+1}^l - W_{i,j}^l) - D_s(W_{i,j}^l - W_{i,j-1}^l)}{\Delta y^2}, \end{aligned}$$

where “ \mathcal{D} ” is for “divergence.” To ensure conservation, $Q_e(u_e)$ used in computing $\mathcal{D}_{i,j}$ must be the same as $Q_w(u_w)$ used in computing $\mathcal{D}_{i+1,j}$, and similarly for “north” and “south” staggered fluxes; our formulas have these properties.

Now our scheme for approximating mass conservation equation (12) is

$$\frac{W_{i,j}^{l+1} - W_{i,j}^l}{\Delta t} + \frac{(W_{\text{til}})_{i,j}^{l+1} - (W_{\text{til}})_{i,j}^l}{\Delta t} = -\mathcal{D}_{i,j} + \frac{m_{ij}}{\rho_w}. \quad (67)$$

The updated value of W_{til} , which appears on the left side of (67), is computed by trivial integration of equation (13), namely

$$(W_{\text{til}})_{i,j}^{l+1} = (W_{\text{til}})_{i,j}^l + \Delta t \left(\frac{m_{ij}}{\rho_w} - C_d \right). \quad (68)$$

The right-hand-side value is used if it is in the closed interval $[0, W_{\text{til}}^{\max}]$, but otherwise the bounds $0 \leq W_{\text{til}} \leq W_{\text{til}}^{\max}$ are enforced. Once W_{til}^{l+1} is computed, the value of W^{l+1} can be updated by (67) in a mass-conserving way.

Assuming no error in the flux components Q , the local truncation error (Morton and Mayers, 2005) of scheme (67) would be $O(\Delta t^1 + \Delta x^2 + \Delta y^2)$ as an approximation of (12). The actual truncation error depends on the nature of the approximation which generates the discrete fluxes; see subsection 9.3 below.

9.3 Discrete advective fluxes

Well-chosen discrete approximations of the advective flux VW are important to the accuracy of the whole scheme. Mass conservation of these schemes essentially follows from using the staggered-grid values as described in the last subsection. In our explicit time-stepping framework we expect, and can show in the simpler first-order case (see next subsection), that stability follows from enforcing a CFL restriction. To examine accuracy, however, we test two flux discretization schemes (67), namely first-order upwind and the Koren flux-limited third-order scheme (Hundsdorfer and Verwer, 2010). Both schemes achieve non-oscillation and positivity, but with different local truncation error and complexity of implementation. The third-order scheme is best explained as a modification of the better-known conservative (“donor cell”; LeVeque (2002)) first-order upwind scheme we use.

In fact, the following formulas apply in the cases $u_e \geq 0$, $u_e < 0$, $v_n \geq 0$, and $v_n < 0$, respectively:

$$\begin{aligned} Q_e(u_e) &= u_e [W_{i,j} + \Psi(\theta_i)(W_{i+1,j} - W_{i,j})], \\ Q_e(u_e) &= u_e [W_{i+1,j} + \Psi((\theta_{i+1})^{-1})(W_{i,j} - W_{i+1,j})], \\ Q_n(v_n) &= v_n [W_{i,j} + \Psi(\theta_j)(W_{i,j+1} - W_{i,j})], \\ Q_n(v_n) &= v_n [W_{i,j+1} + \Psi((\theta_{j+1})^{-1})(W_{i,j} - W_{i,j+1})]. \end{aligned} \quad (69)$$

The subscripted θ quotients are as follows:

$$\begin{aligned} \theta_i &= \frac{W_{i,j} - W_{i-1,j}}{W_{i+1,j} - W_{i,j}}, & (\theta_{i+1})^{-1} &= \frac{W_{i+2,j} - W_{i+1,j}}{W_{i+1,j} - W_{i,j}}, \\ \theta_j &= \frac{W_{i,j} - W_{i,j-1}}{W_{i,j+1} - W_{i,j}}, & (\theta_{j+1})^{-1} &= \frac{W_{i,j+2} - W_{i,j+1}}{W_{i,j+1} - W_{i,j}}. \end{aligned}$$

The first-order upwind scheme simply sets $\Psi(\theta) = 0$ in formulas (69). The Koren scheme “limits” its third-order and positive-coefficient correction to the upwind scheme by using this formula (Hundsdorfer and Verwer, 2010):

$$\Psi(\theta) = \max \left\{ 0, \min \left\{ 1, \theta, \frac{1}{3} + \frac{1}{6}\theta \right\} \right\}. \quad (70)$$

Thus one does not compute θ quotients at all when using first-order upwind. On the other hand, when using the Koren flux-limiter the stencil in Figure 6 is extended because regular grid neighbors $W_{i+2,j}$, $W_{i-2,j}$, $W_{i,j+2}$, $W_{i,j-2}$ are also involved in updating $W_{i,j}$.

The flux-correction-limited Koren third-order scheme bypasses the first-order limitation of positive linear finite difference/volume schemes imposed by Godunov’s barrier theorem (Hundsdorfer and Verwer, 2010, section I.7.1) by having a nonlinear correction formula, i.e. the combination of (69) and (70) above. Though the Koren scheme is usually third-order where smoothness allows, it reverts to first-order at extrema and other non-smooth areas where $\theta \gg 1$ or $\theta \ll 1$.

For either the first-order or Koren schemes, if the water input m is negative then we must actively enforce the positivity of the water thickness W . Positivity of the source-free

advection-diffusion scheme is a desirable property but it does not ensure positivity of the solution if there is actual water removal (i.e. if $(m/\rho_w) - \partial W_{\text{til}}/\partial t < 0$). Therefore we project (reset) W to be nonnegative at the end of each time step.

9.4 Mass conservation: positivity and stability

Explicit numerical scheme (67) for the mass conservation PDE (12), combined with the first-order upwind case of formulas (69), is sufficiently simple so that we can analyze its stability properties. For this scheme we now sketch a maximum principle argument which shows stability (Morton and Mayers, 2005). The argument also shows positivity (Hundsdorfer and Verwer, 2010) as long as the total water input is nonnegative, but here only the case $m = 0$ and $W_{\text{til}}^{\max} = 0$ case is shown. Also we consider only the upwinding case where the discrete velocities at cell interfaces are nonnegative: $u_e \geq 0$, $u_w \geq 0$, $v_n \geq 0$, $v_s \geq 0$. The other upwinding cases can be handled by similar arguments.

Define $\nu_x = \Delta t/\Delta x$, $\nu_y = \Delta t/\Delta y$, $\mu_x = \Delta t/\Delta x^2$, and $\mu_y = \Delta t/\Delta y^2$. Collecting terms in (67) to write the new value as a linear combination of the old values, we get

$$\begin{aligned} W_{i,j}^{l+1} &= (\nu_x u_w + \mu_x D_w) W_{i-1,j}^l + (\mu_x D_e) W_{i+1,j}^l \\ &\quad + (\nu_y v_s + \mu_y D_s) W_{i,j-1}^l + (\mu_y D_n) W_{i,j+1}^l \\ &\quad + \left[1 - \nu_x u_e - \nu_y v_n - \mu_x (D_e + D_w) - \mu_y (D_n + D_s) \right] W_{i,j}^l \\ &= \tilde{A} W_{i-1,j}^l + \tilde{B} W_{i+1,j}^l + \tilde{C} W_{i,j-1}^l \\ &\quad + \tilde{D} W_{i,j+1}^l + \tilde{E} W_{i,j}^l. \end{aligned} \quad (71)$$

Because of our assumption about nonnegative velocities, and noting that the diffusivities are nonnegative, we see that coefficients $\tilde{A}, \tilde{B}, \tilde{C}, \tilde{D}$ are all nonnegative. Only \tilde{E} could be negative, depending on values of ν_x, ν_y, μ_x , and μ_y .

Requiring \tilde{E} in (71) to be nonnegative is a sufficient stability condition (Morton and Mayers, 2005), which we generate based on an equal split between advective and diffusive parts. First there is a CFL restriction for the advection terms, namely $\nu_x \alpha_e + \nu_y \beta_n \leq \frac{1}{2}$, which is condition (60) when generalized to all upwinding cases. The second is a time-step restriction on the diffusion, namely $\mu_x (D_e + D_w) + \mu_y (D_n + D_s) \leq \frac{1}{2}$, which is condition (61). If both (60) and (61) hold then the coefficient \tilde{E} in (71) is nonnegative.

Because the coefficients in linear combination (71) also add to one, as the reader may check, it follows from (60) and (61) that the scheme is stable (Morton and Mayers, 2005). It also follows from (60) and (61) that if $W_{i,j}^l \geq 0$ for all i, j then (71) gives $W_{i,j}^{l+1} \geq 0$, in this $m = 0$ and $W_{\text{til}}^{\max} = 0$ case, which is our positivity claim. Thus, under conditions (60) and (61), scheme (67) is stable and positivity-preserving.

9.5 Discretization of the pressure equation

The pressure evolution equation (34) is a nonlinear diffusion with additional “reaction” terms associated to opening and closing. The time step restriction for our explicit pressure scheme is comparable to (61), though the proof above for the stability of the mass conservation scheme does not suffice to prove stability. That is, if the time step satisfies $\Delta t \leq \Delta t_P$, where

$$\Delta t_P \left(\frac{2 \max D}{\phi_0} \right) \left(\frac{1}{\Delta x^2} + \frac{1}{\Delta y^2} \right) = 1 \quad (72)$$

then we assert that, and observe in practice that, the scheme is stable. From (61) the resulting time step Δt_P is a fraction of Δt_W :

$$\Delta t_P = 2\phi_0 \Delta t_W. \quad (73)$$

We can again be quantitative in a particular example. Consider the same 250 m simulation of the hydrology of Norden-skioldbreen as earlier. With $\phi_0 = 0.01$ we have Δt_P which is 50 times smaller than Δt_W and half of Δt_{CFL} :

$\Delta t_W \approx 8000$ s	from (61),
$\Delta t_{\text{CFL}} \approx 300$ s	from (60),
$\Delta t_P \approx 160$ s	from (73).

This analysis suggests that the numerical scheme for pressure diffusion, given next, may often have the shortest time step, but it may be comparable to CFL. Note that $\Delta t_{\text{CFL}} = O(\Delta x)$ while Δt_W and Δt_P are $O(\Delta x^2)$. The time step restriction Δt_P scales with the adjustable regularizing porosity ϕ_0 so we can make it more or less severe.

The scheme we use for the pressure equation (34) is similar to the scheme we have just presented for the mass continuity equation (12). Denote $\psi_{i,j}^l = P_{i,j}^l + \rho_w g(b_{i,j}^l + W_{i,j}^l)$. Let $\mathcal{O}_{ij} = c_1 |\mathbf{v}_b|_{i,j} (W_r - W_{i,j}^l)_+$ and $\mathcal{C}_{ij} = c_2 A (\rho_i g H_{i,j} - P_{i,j}^l)^3 W_{i,j}^l$ be the gridded values of the cavitation-opening and creep-closure rates. Also define the sum of all zero order (i.e. without spatial derivatives) terms

$$Z_{ij} = \mathcal{C}_{ij} - \mathcal{O}_{ij} + \frac{m_{ij}}{\rho_w} - \frac{(W_{\text{til}})_{ij}^{l+1} - (W_{\text{til}})_{ij}^l}{\Delta t}. \quad (74)$$

Using (66) for the flux divergence, the scheme for pressure equation (34) is now

$$\frac{\phi_0}{\rho_w g} \frac{P_{i,j}^{l+1} - P_{i,j}^l}{\Delta t} = -\mathcal{D}_{i,j} + Z_{ij}, \quad (75)$$

or, in explicit update form,

$$P_{i,j}^{l+1} = P_{i,j}^l + \frac{\rho_w g \Delta t}{\phi_0} (-\mathcal{D}_{i,j} + Z_{ij}). \quad (76)$$

Because equation (74) uses the updated value $(W_{\text{til}})_{ij}^{l+1}$, equation (68) must be applied before (76) can be used to update P to the new time t_{l+1} .

There are special cases at the boundaries of the active subglacial layer: (i) where there is no ice $H_{i,j} = 0$ and land ($b_{i,j} > 0$) we set $P_{i,j}^{l+1} = 0$, (ii) where the ice is floating we set $P_{i,j}^{l+1} = (P_o)_{i,j}$, and (iii) where there is grounded ice ($H_{i,j} > 0$) and no water ($W_{i,j}^l = 0$) we set $P_{i,j}^{l+1} = (P_o)_{i,j}$ if there is no basal sliding and $P_{i,j}^{l+1} = 0$ if there is sliding (because of cavitation; see equation (46)).

9.6 One time step of the model

Mathematical model (35) evolves W , W_{til} , and P . Here we describe one time step of the fully-discretized evolution. For convenience we treat the ice geometry and sliding speed as fixed, and so $h_{i,j}$, $b_{i,j}$, $(P_o)_{i,j}$, and $|\mathbf{v}_b|_{i,j}$ are all denoted as time-independent.

The ice geometry may be quite general, with ice-free land or floating ice allowed at any location (x_i, y_j) . The ice geometry determines boolean “masks” for grid cell state (based on zero sea level elevation):

$$\begin{aligned} \text{icefree}_{i,j} &= (h_{i,j} > 0) \& (h_{i,j} = b_{i,j}), \\ \text{float}_{i,j} &= (\rho_i (H_{\text{float}})_{i,j} < -\rho_{sw} b_{i,j}). \end{aligned}$$

Here we take a sea-water density $\rho_{sw} = 1028.0$ and $H_{\text{float}} = h_{i,j}/(1-r)$ is the thickness of the ice if it is floating, where $r = \rho_i/\rho_{sw}$. Note that $\text{float}_{i,j}$ is also true in ice-free ocean. The subglacial hydrology model exists only for grounded ice, that is, only if both icefree and float are false. The other mask cases provide boundary conditions when they are neighbors to grounded ice-filled cells.

One time step follows this algorithm:

- (i) Start with values $W_{i,j}^l$, $(W_{\text{til}})_{i,j}^l$, $P_{i,j}^l$ which satisfy the bounds $W \geq 0$, $0 \leq W_{\text{til}} \leq W_{\text{til}}^{\text{max}}$, and $0 \leq P \leq P_o$.
- (ii) Get $(W_{\text{til}})_{i,j}^{l+1}$ by (68). If $\text{icefree}_{i,j}$ or $\text{float}_{i,j}$ then set $(W_{\text{til}})_{i,j}^{l+1} = 0$.
- (iii) Get W values averaged onto the staggered grid from (62), staggered grid values of the effective conductivity K from (63), velocity components u , v at staggered grid locations from (64), and staggered grid values of the diffusivity D from (65).
- (iv) Get time step $\Delta t = \min\{\Delta t_{\text{CFL}}, \Delta t_W, \Delta t_P\}$ using criteria (60), (61), and (73), based on the current staggered-grid values of u , v , and D .
- (v) Using (69) and a particular flux-limiter, compute the advective fluxes $Q_e(\alpha_e)$ at all staggered-grid points $(i+1/2, j)$ and $Q_n(\beta_n)$ at all staggered-grid points $(i, j+1/2)$.

(vi) Get approximations $\mathcal{D}_{i,j}$ of the flux divergence from (66). For each direction (i.e. x - and y -directions), do not compute the divided-difference contribution to the flux divergence in (66) if either neighbor is `icefree` or `float`.
1410

(vii) If `icefreei,j` then set $P_{i,j}^{l+1} = 0$. If `floati,j` then set $P_{i,j}^{l+1} = (P_o)_{i,j}$. If $W_{i,j}^l = 0$ and `icefreei,j` and `floati,j` are both false, then set $P_{i,j}^{l+1} = (P_o)_{i,j}$. Then use (76) to compute values for $P_{i,j}^{l+1}$ at the remaining locations.
1420

(viii) If $P_{i,j}^{l+1}$ does not satisfy bounds $0 \leq P \leq P_o$ then reset (project) into this range.
1430

(ix) If `icefreei,j` or `floati,j` then set $W_{i,j}^{l+1} = 0$. Otherwise use (67) to compute values for $W_{i,j}^{l+1}$.

(x) If $W_{i,j}^{l+1} < 0$ then reset (project) $W_{i,j}^{l+1} = 0$.

(xi) Update time $t_{l+1} = t_l + \Delta t$ and repeat at (i).
1440

This recipe goes with a reporting scheme for mass conservation. Note that in steps (ii) and (ix) water is lost or gained at the margin where either the ice thickness goes to zero on land (margins), or at locations where the ice becomes floating (grounding lines). Because such loss/gain may be the modeling goal—users want hydrological discharge—these amounts are reported. This reporting scheme also tracks the projections in step (x), which represent a mass conservation error which goes to zero under the continuum limit $\Delta t \rightarrow 0$.
1450

10 PISM options for hydrology models

In this section we document the runtime options for the PISM hydrology model (PISM authors, 2013). There are three choices of model equations, namely `distributed`, `routing`, and `null`. The first of these is the complete model described in this paper. The other two are reductions; we list them in order of decreasing complexity. We also give a concordance between the symbols in this paper and the relevant PISM configuration parameters.
1460

10.1 distributed

This most-complete PISM hydrology model is chosen by runtime option `-hydrology distributed`. It is governed by the full set of equations (35) in section 6; see also Tables 1 and 2.
1470

10.2 routing

This model is chosen by option `-hydrology routing`. It is governed by a subset of equations (35), with the equation for evolution of pressure P removed, and with the replacement $P \mapsto P_o = \rho_i g H$ in defining K , \mathbf{V} , and ψ . Thus
1480

the equations simplify to:

$$\begin{aligned} \frac{\partial W}{\partial t} + \frac{\partial W_{\text{til}}}{\partial t} &= -\nabla \cdot (\mathbf{V} W) + \nabla \cdot (D \nabla W) + \frac{m}{\rho_w}, \\ \frac{\partial W_{\text{til}}}{\partial t} &= \frac{m}{\rho_w} - C_d, \\ \tau_c &= c_0 + (\tan \varphi) N_{\text{til}}, \\ N_{\text{til}} &= \min \left\{ P_o, N_0 \left(\frac{\delta P_o}{N_0} \right)^s 10^{(e_0/C_c)(1-s)} \right\}, \end{aligned} \quad (77)$$

along with $s = W_{\text{til}}/W_{\text{til}}^{\max}$ and the bounds $0 \leq W$ and $0 \leq W_{\text{til}} \leq W_{\text{til}}^{\max}$.

10.3 null

This non-conserving model is chosen by option `-hydrology null`. It is the default hydrology model in PISM. It has only the state variable W_{til} . The determination of basal yield stress is unchanged. The equations are the same as in (77) except that there is no “ W ” and the first of equations (77) is gone. Bounds $0 \leq W_{\text{til}} \leq W_{\text{til}}^{\max}$ remain.

10.4 PISM configuration variables

All of the constants in Table 2 are configurable parameters in PISM. The correspondence between PISM parameters names and the symbols in this paper is in Table 4. These parameters can be changed at runtime by using the parameter name as an option or by setting a `pism_overrides` variable in a NetCDF file which is read with the `-config_override` option. See `src/pism_config.cdl` for default values and units.

11 Results

11.1 Verification of the coupled model

By using the coupled steady-state exact solution constructed in section 8 we can verify most of the numerical schemes described above. Verification is the process of measuring and analysing the errors made by the numerical scheme, especially as the numerical grid is refined (Wesseling, 2001; Bueler et al., 2005).

The exact solution described in subsection 8.2, and shown in Figures 4 and 5, is for steady-state. We initialize our time-stepping numerical scheme with the exact steady solution and we measure the error relative to the steady exact values after some period of time integration. The continuum time-dependent model (35) would cause no drift away from steady state, so any drift is error.

For the verification runs we use the values in Table 3. We do one model-month runs on grids decreasing by factors of two from 2 km to 125 m. Figure 7 shows the results based on first-order upwinding for the fluxes.

Table 4. Correspondence between symbols in this paper and PISM configuration parameter names. Alphabetical by parameter name. All of these are used in the distributed model, with the indicated subsets also used in the routing and null models.

PISM configuration name	Symbol	routing	null
fresh_water_density	ρ_w	×	×
hydrology_cavitation_opening_coefficient	c_1		
hydrology_creep_closure_coefficient	c_2		
hydrology_gradient_power_in_flux	β	×	
hydrology_hydraulic_conductivity	k	×	
hydrology_regularizer_porosity	ϕ_0		
hydrology_roughness_scale	W_r		
hydrology_thickness_power_in_flux	α	×	
hydrology_tillwat_decay_rate	C_d	×	×
hydrology_tillwat_max	W_{til}^{\max}	×	×
ice_density	ρ_i	×	×
ice_softness	A		
standard_gravity	g	×	×
till_c_0	c_0	×	×
till_compressibility_coefficient	C_c	×	×
till_effective_fraction_overburden	δ	×	×
till_reference_effective_pressure	N_0	×	×
till_reference_void_ratio	e_0	×	×

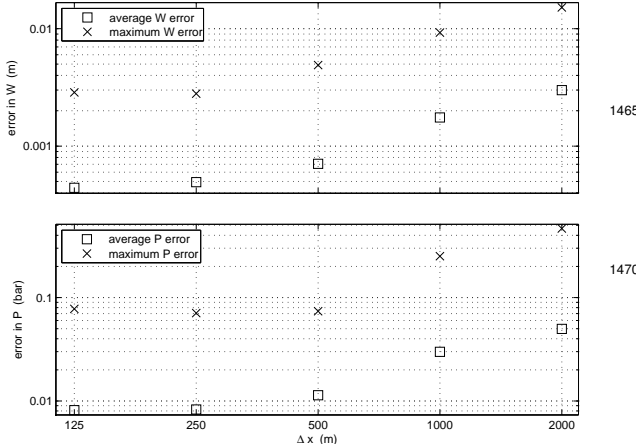


Fig. 7. Average water thickness error $|W - W_{\text{exact}}|$ decays as $O(\Delta x^{0.91})$, and average pressure error $|P - P_{\text{exact}}|$ decays as $O(\Delta x^{0.92})$, for grids with spacing $250 \leq \Delta x = \Delta y \leq 2000$ m.

This convergence evidence suggests that the coupled advection-diffusion-reaction equations for W and P have correctly-implemented numerical schemes. The rate of convergence is roughly linear (i.e. about $O(\Delta x^1)$) because largest errors arise at locations of low regularity of the solution, including the radius $r = R_1$ where P abruptly drops from P_o , and at the ice sheet margin $r = L$ where there is a jump in the water thickness to zero.

The rates of convergence for average errors are nearly identical for the higher resolution flux-limited (Koren) scheme and for the first-order upwinding scheme (not

shown). Because our problem is an advection-diffusion problem in which both the advection velocity and the diffusivity are solution-dependent, it is difficult to separate the errors arising from numerical treatments of advection and diffusion. The first-order upwinding scheme for the advection has much larger numerical diffusivity but this diffusivity is masked by the physical diffusivity. Based on our verification evidence it is reasonable to choose the simpler first-order upwinding for applications. It also requires less interprocess communication in our parallel implementation.

11.2 Application of the model at ice sheet scale

11.2.1 Spun-up initial state

We have applied our mass-conserving hydrology models to the entire present-day Greenland ice sheet at 2 km resolution. This serves as a nontrivial example showing the implementability of the model at large computational scale with high resolution using real data, and of one-way coupling with ice dynamics. For simplicity and consistency with prior work, the present-day state of the ice sheet, especially data for the ice thickness, surface mass balance, and surface temperature, were taken from the SeaRISE data set for Greenland (Bindschadler et al., 2013; Nowicki et al., 2013; and references therein).

The PISM ice dynamics and thermodynamics model (Bueler and Brown, 2009; Winkelmann et al., 2011; Aschwanden et al., 2012), using the non-mass-conserving null hydrology model (section 10), was applied by grid sequencing to compute a consistent and nearly-steady model

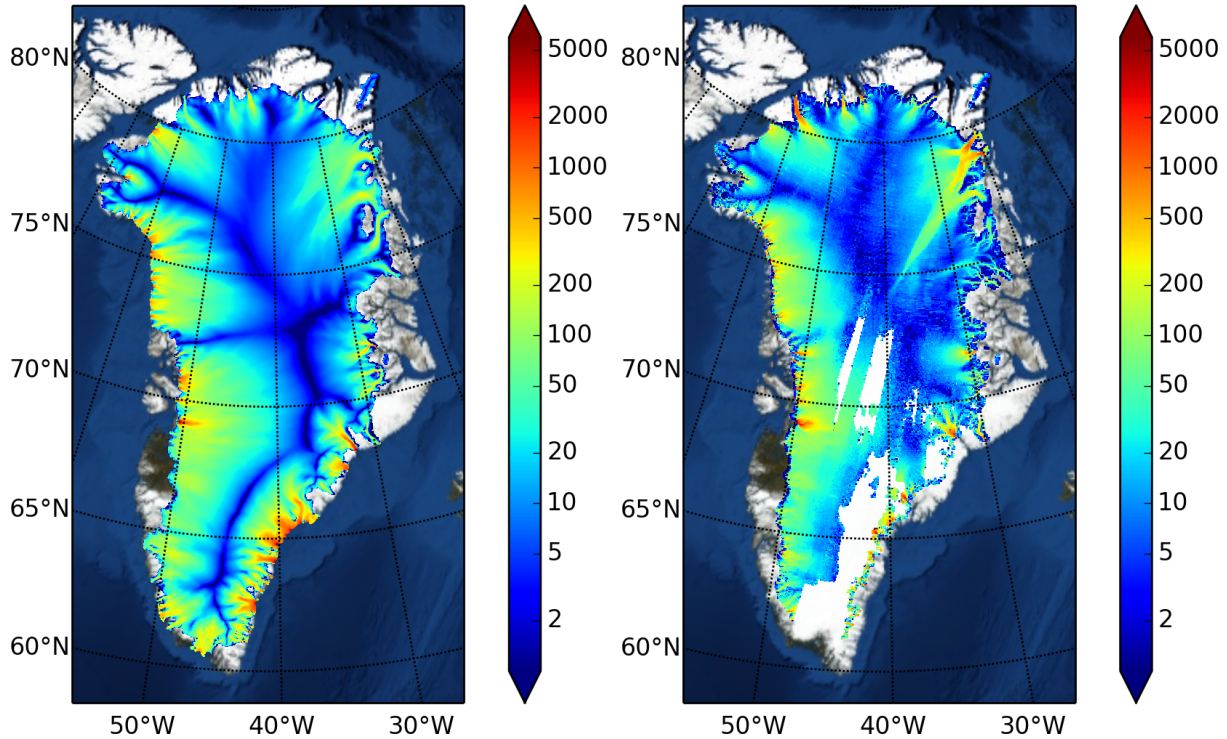


Fig. 8. To evaluate the result of the 2 km grid spun-up ice dynamical model we compare modelled ice speed at the ice surface (left; m a^{-1}) to satellite observations (right; m a^{-1}).

of the ice sheet, a “spun-up” initial state. Model choices for ice dynamics, including enhancement factor, sliding law power, and the model for till friction angle, followed those in Aschwanden et al. (2013). The present-day climate including surface temperature and mass balance was from (Ettema et al., 2009). The grid sequence was to run for 50 ka on a 20 km grid, 20 ka on a 10 km grid, 2 ka on a 5 km grid, and finally 200 a on a 2 km grid, with bilinear interpolation of all model fields at each refinement stage. This whole spinup used 2800 processor-hours on parallel runs of 72 processors on a linux cluster using 2.2 GHz AMD Opteron Processors. (This represents a small computation for modern clusters which may have more than 100k processors.)

The final 2 km stage, on a horizontal grid of 1.05 million grid points, used uniform 10 m vertical spacing so that the ice sheet flow was modelled on a structured 3D grid of 460 million grid points (e.g. locations where ice temperature and velocity were computed). In the last 100 a of the final stage the ice sheet volume varied by less than 0.04 percent. Other more active measures showed stability during the last 100 a at the level of less than one percent (e.g. the area of temperate base and the maximum ice velocity over the whole sheet) to at most a few percent (the floating ice area).

The results of this whole-ice-sheet spinup were validated by comparing results to present-day observations. Though the model is in nearly steady state, the actual ice sheet may not be as close to steady. The spun-up ice sheet volume

of $3.094 \times 10^6 \text{ km}^3$ is close to the present-day volume of $3.088 \times 10^6 \text{ km}^3$ computed from the SeaRISE data on the same grid. However, in describing more careful validation measures for similar 2 km PISM model runs, Aschwanden et al. (2013) observe that volume alone is inadequate for model validation. A better evaluation of dynamical quality is shown in Figure 8, which compares the modeled and observed surface speed. We see that, the extent of the Northeast Greenland ice stream is smaller than observed, and the distribution of flow in Western Greenland outlet glaciers differs from the observed pattern. Our model uses no spatially-variable parameter values such as basal shear stresses found by inversion of surface velocities.

The spun-up initial state includes, in particular, modelled ice thickness H , basal melt rate m , and sliding velocity $|\mathbf{v}_b|$; the latter two fields are shown in Figure 9. We note that the areas of sliding roughly coincide with areas of basal melt because modeled basal resistance comes from the yield stress parameterized in section 3.

11.2.2 Experimental setup

We then used the fields H , m , $|\mathbf{v}_b|$ as steady data in five model-year runs of our mass-conserving hydrology routing and distributed models. Because these fields were fixed, only one-way coupling is tested here. That is, a steady ice dynamics model fed its fields to an evolving sub-

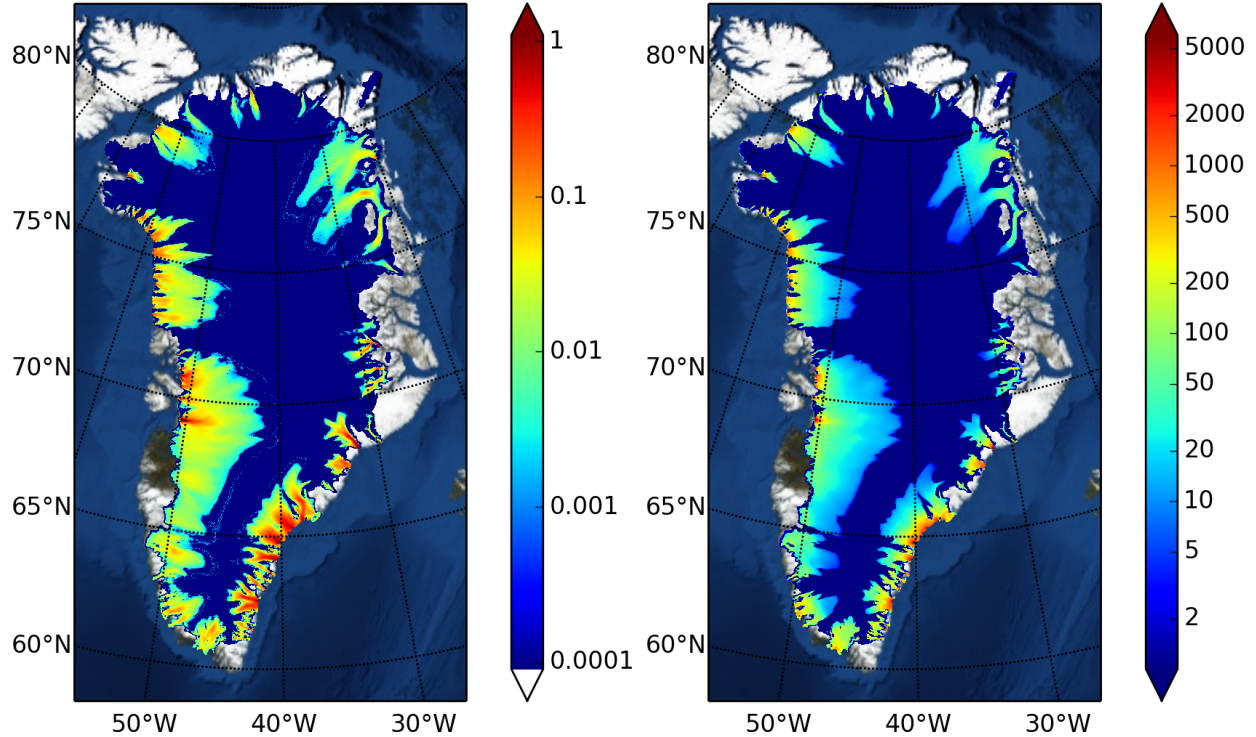


Fig. 9. The inputs to the hydrology model are the modeled basal melt rate m/ρ_w (left; m a^{-1}) and sliding speed $|\mathbf{v}_b|$ (right; m a^{-1}) from the spun-up model.

glacial hydrology model. The hydrology model was initialized with the W_{til} values from the spun-up state, but with $W = 0$ initial values (for both models) and $P = 0$ initial values (for distributed).

These runs had 1.05 million subglacial hydrology grid points at which variables W , W_{til} , and P were recomputed at each time-step according to the numerical model described in section 9. In both `routing` and `distributed` models the modelled hydrological system became quite steady after the first three model years. The adaptively-determined time-steps for the hydrology model reached a steady level of 4 model hours for the `routing` model based on maximum subglacial water speeds $|\mathbf{V}|$ of 0.05 m s^{-1} and maximum diffusivity D of $10.6 \text{ m}^2 \text{s}^{-1}$. For the complete `distributed` model the time steps were actually slightly longer than 1570 1575 1580 1585 1590 1595 1599 routing primarily because the `routing` model concentrates large water amounts, and thus fluxes, along steepest-descent paths. In the `distributed` model the time steps were about 6 model hours based on speeds $|\mathbf{V}|$ of 0.03 m s^{-1} and substantially-smaller maximum diffusivities of about D of $0.25 \text{ m}^2 \text{s}^{-1}$. (Note comments on the actual diffusivity of advective fluxes in section 7. Also, higher water velocities \mathbf{V} were seen in the Nordenskiöldbreen case in section 9, based on additional simulated surface water input added to the thermodynamically-generated basal melt rate (van Pelt, 1590 1593 2013). In that tidewater glacier case the pressure-evolution

time-steps are seen to be substantially shorter than the mass-conservation time steps.)

11.2.3 routing results

The final values of W_{til} and W for the `routing` run are shown in Figure 10. We see that the till is fully saturated ($W_{\text{til}} = 2 \text{ m}$) in essentially all areas where basal melt occurs. In the outlet glacier areas the transportable water W concentrates along curves of steepest descent of the hydraulic potential; this effect is seen in detail in Figure 11. The grid resolution of 2 km, while very high for contemporary ice dynamics models, still represents a significant spatial “smearing” of the flow pathways. Specifically, though relatively few areas have $W > 1$, the continuum limit of the model would be expected to have $W \gg 1$ in concentrated pathways of a few meters to tens of meters width. These effects are seen in detail in Figure 11.

On the one hand this model could be regarded as a minimal “conduit-like” description of the subglacial flow, because of these model concentrated pathways. On the other hand, as noted in the introduction, there is no “R-channel” mechanism used in this paper; in that mechanism the dissipation heating of the flowing water would generate wall melt-back to hold the channel open. Thus the time-dependence and flux magnitudes in the model are not “R-channel”-like. At a more basic level, the authenticity of subglacial “channel” geometry here

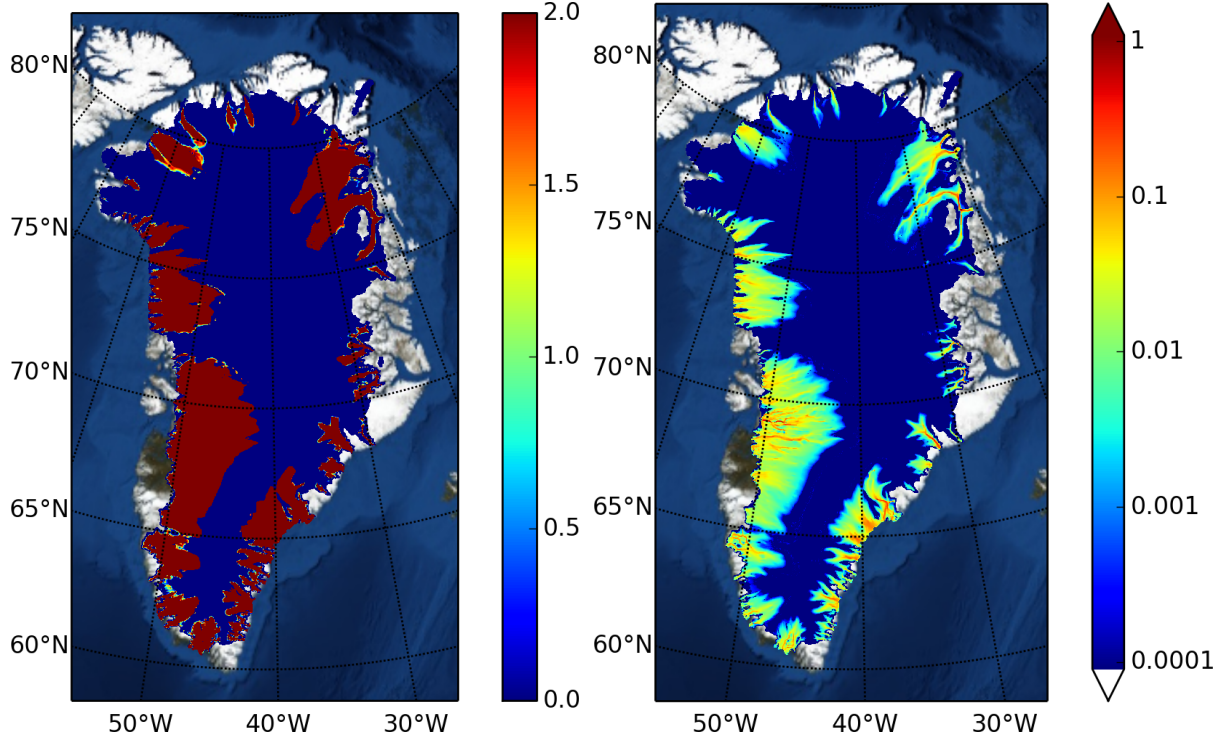


Fig. 10. Outputs from the routing hydrology model are the modelled till-stored water layer thickness W_{til} (left; m) and modelled transportable water layer thickness W (right; m).

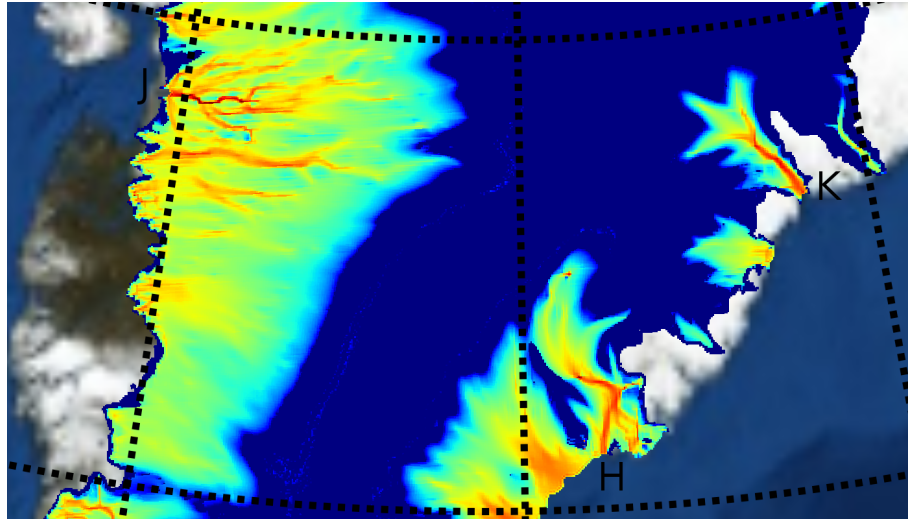


Fig. 11. Detail of transportable water W plotted in Figure 10, covering Jakobshavn (J), Helheim (H), and Kangerdlugssuaq (K) outlet glaciers

is determined primarily by the bedrock elevation detail provided by the SeaRISE data set, which is limited; this effect is severe in the Eastern outlet glaciers (Helheim and Kangerdlugssuaq) shown in Figure 11.

11.2.4 distributed results

The final values of W and the relative water pressure P/P_o for the five model-year distributed run are shown in Figure 12. Again the till is full ($W_{\text{til}} = W_{\text{til}}^{\max} = 2 \text{ m}$) in essentially all areas where basal melt occurs, so W_{til} is not shown because it is identical to that in the routing model in this

one-way coupled case. (Note the simple W_{til} evolution equation given in section 4.)

Recall that $|\mathbf{v}_b|$ determines the pressure drop caused by cavitation. The tendency of this effect to spread out the water W , relative to the routing model, is clearly seen in the distributed results in Figure 12. There is no strong concentration of W along curves of steepest descent of the hydraulic potential. This result is strongly dependent on the opening and closing parameters in the distributed model, especially parameters c_1, c_2, ϕ_0, W_r ; see Tables 2 and 4. (These are in addition to the Darcy flux model parameters α, β, k already used in the routing model.) Parameter identification through observed data is obviously needed, but it is beyond the scope of the current paper.

As a final observation about the distributed model results, we examine the local relationship between water amount W and pressure P . Though the model is near steady state, the basal melt rate, sliding speed, and overburden pressure all show the large spatial variations which are characteristic of a real ice sheet.

Figure 13 shows that if we “bin” pairs (W, P) by relatively-narrow sliding velocity ranges, as shown in each scatter plot, then there is usually a rough increasing relationship between W and the relative pressure P/P_o . Recall that in exact steady state the equation (46) applies; see also Figures 2 and 3. At fast-sliding locations the water amount is often comparable to the bed roughness scale W_r . For low sliding velocities we see generally lower water amounts ($W \lesssim W_r/10$) but a full range of pressures. Furthermore we can observe that in thick ice with high overburden pressure the pressure P is close to overburden even if there is fast sliding. Locations with high sliding, high water amount, and low pressure also have low ice thickness. Figure 13 would show even more scatter if the run were not close to steady state, such as if there were time-varying surface melt input into the subglacier (van Pelt, 2013).

It would be possible to implement a model without a pressure evolution equation like (34), and instead use (46) as a prescribed relation $P(W)$. However, we prefer such a local relationship to “emerge” in steady state, as here. Tests of the model with time-dependent inputs clearly suggest the importance of a full pressure evolution equation to modeling response to a seasonal surface melt cycle (van Pelt, 2013).

12 Conclusions

The literature of subglacial hydrology modeling has grown rapidly in the last five years. In this context the current paper, which documents additions made to the Parallel Ice Sheet Model in its 0.6 version released February 2014, is both novel and comprehensive, despite primarily describing the details of a PISM submodel. It is novel in these features:

- parallel implementation in two horizontal dimensions at scale (sections 9 and 11) of a coupled till-and-linked-cavities model,
- a new analysis of steady state explaining the degree to which a functional relationship $P(W)$ is justified (section 7),
- an exact solution of the coupled mass and pressure equations of the distributed model in the steady angularly-symmetric case (section 7), plus verification using this solution (section 11), and
- an englacial porosity regularization which is shown to allow a practical numerical model in which physically-motivated bounds $0 \leq P \leq P_o$ hold at all times (sections 4, 5, and 9).

We believe, however, that the comprehensive treatment here of certain subjects is also important. We assert that

- we have clarified the relationship of several “closures” which turn morphological ideas about the subglacial aquifer into concrete pressure equations (section 5), and
- we have implemented a common extension of several seemingly-disparate published models (section 6).

On the other hand, a deliberate limitation in scope of the current paper is that we demonstrate only one-way coupling: the PISM ice flow and thermodynamics model feeds basal melt rate and sliding speed values to the hydrology model. Two-way coupling in a high-resolution model for the whole of the Greenland ice sheet will appear in future work.

Acknowledgements. The first author was supported by NASA grant #NNX13AM16G. This work was supported by a grant of high-performance computing resources from the Arctic Region Supercomputing Center. Constantine Khroulev helped with the PISM implementation. Discussions with, and detailed comments by, Andy Aschwanden, Tim Bartholomaus, and Martin Truffer were much appreciated.

References

- Ascher, U. and Petzold, L.: Computer Methods for Ordinary Differential Equations and Differential-algebraic Equations, SIAM Press, Philadelphia, PA, 1998.
- Aschwanden, A., Bueler, E., Khroulev, C., and Blatter, H.: An enthalpy formulation for glaciers and ice sheets, *J. Glaciol.*, 58, 441–457, doi:10.3189/2012JoG11J088, 2012.
- Aschwanden, A., Adalgeirsdóttir, G., and Khroulev, C.: Hindcasting to measure ice sheet model sensitivity to initial states, *The Cryosphere*, 7, 1083–1093, doi:10.5194/tc-7-1083-2013, 2013.
- Balay, S. et al.: PETSc Users Manual, Tech. Rep. ANL-95/11 - Revision 3.2, Argonne National Laboratory, 2011.
- Bartholomaus, T. C., Anderson, R. S., and Anderson, S. P.: Response of glacier basal motion to transient water storage, *Nature Geosci.*, 1, 33–37, doi:10.1038/ngeo.2007.52, 2008.

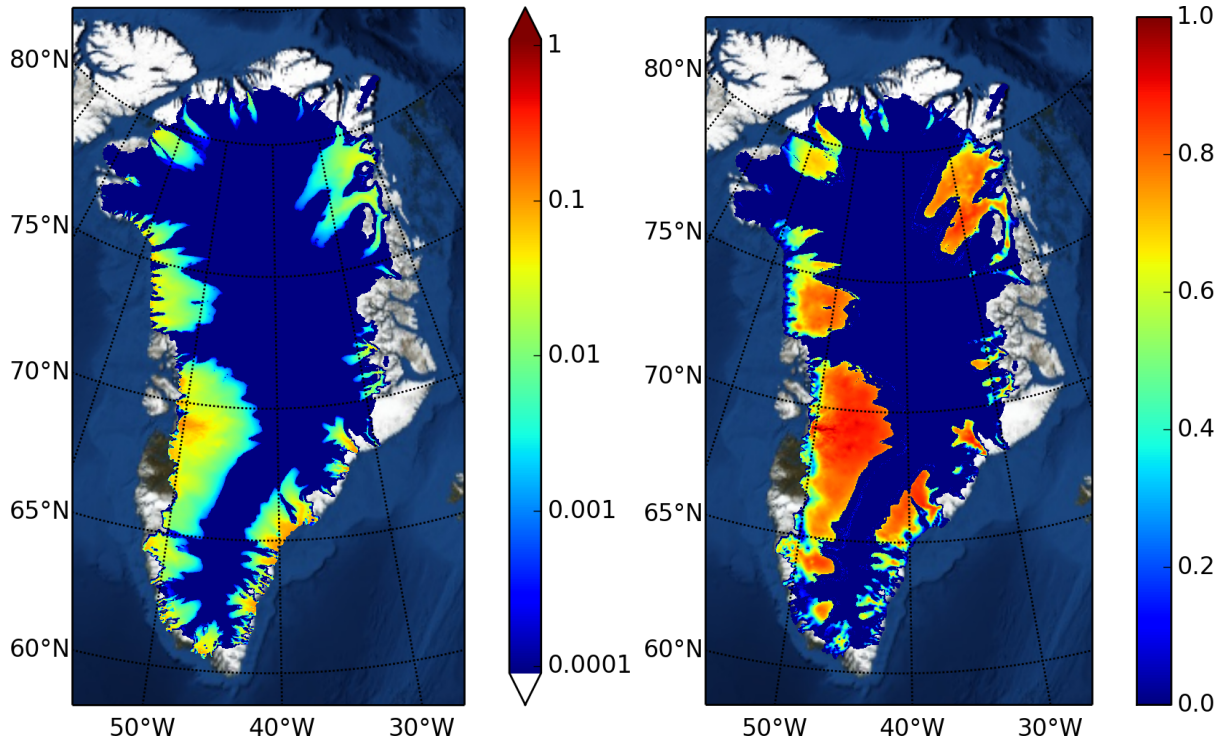


Fig. 12. Outputs from the distributed hydrology model are the modelled till-stored water layer thickness W_{til} (not shown because it is identical to the result from the routing model in this case; see text), the modelled transportable water layer thickness W (left; m), and the modelled transportable water layer pressure relative to overburden pressure P/P_o (right).

Bartholomaus, T. C., Anderson, R. S., and Anderson, S. P.: Growth₁₇₃₀ and collapse of the distributed subglacial hydrologic system of Kennicott Glacier, Alaska, USA, and its effects on basal motion, *J. Glaciol.*, 57, 985–1002, 2011.

1705 Bindschadler, R. et al.: Ice-sheet model sensitivities to environmental forcing and their use in projecting future sea-level (The₁₇₃₅ SeaRISE Project), *J. Glaciol.*, 59, 195–224, 2013.

Bueler, E.: Correspondence: Extensions of the lumped subglacial-englacial hydrology model of Bartholomaus, et al. (2011), submitted to *J. Glaciol.*, 2014.

Bueler, E. and Brown, J.: Shallow shelf approximation as a “sliding₁₇₄₀ law” in a thermodynamically coupled ice sheet model, *J. Geophys. Res.*, 114, f03008, doi:10.1029/2008JF001179, 2009.

1715 Bueler, E. et al.: Exact solutions and numerical verification for isothermal ice sheets, *J. Glaciol.*, 51, 291–306, 2005.

Clarke, G. K.: Hydraulics of subglacial outburst floods: new insights₁₇₄₅ from the Spring-Hutter formulation, *J. Glaciol.*, 49, 299–313, doi:10.3189/172756503781830728, 2003.

1720 Clarke, G.: Subglacial processes, *Annu. Rev. Earth Planet. Sci.*, 33, 247–276, doi:10.1146/annurev.earth.33.092203.122621, 2005.

Creys, T. and Schoof, C.: Drainage through subglacial water sheets,₁₇₅₀ *J. Geophys. Res.*, 114, doi:10.1029/2008JF001215, 2009.

1725 Cuffey, K. M. and Paterson, W. S. B.: *The Physics of Glaciers*, Elsevier, 4th edn., 2010.

Das, S. B., Joughin, I., Behn, M. D., Howat, I. M., King, M. A., Lizarralde, D., and Bhatia, M. P.: Fracture Propagation to the₁₇₅₅ Base of the Greenland Ice Sheet During Supraglacial Lake Drainage, *Science*, 320, 778–781, doi:10.1126/science.1153360,

2008.

de Fleurian, B., Gagliardini, O., Zwinger, T., Durand, G., Le Meur, E., Mair, D., and Råback, P.: A double continuum hydrological model for glacier applications, *The Cryosphere*, 8, 137–153, doi:10.5194/tc-8-137-2014, 2014.

Ettema J. et al.: Higher surface mass balance of the Greenland ice sheet revealed by high-resolution climate modeling, *Geophys. Res. Lett.*, 36, L12501, doi:10.1029/2009GL038110, 2009.

Evans, L. C.: *Partial Differential Equations*, Graduate Studies in Mathematics, American Mathematical Society, 1998.

Flowers, G. E. and Clarke, G. K. C.: A multicomponent coupled model of glacier hydrology 1. Theory and synthetic examples, *J. Geophys. Res.*, 107, 2287, doi:10.1029/2001JB001122, 2002a.

Flowers, G. E. and Clarke, G. K. C.: A multicomponent coupled model of glacier hydrology 2. Application to Trapridge Glacier, Yukon, Canada, *J. Geophys. Res.*, 107, 2288, doi:10.1029/2001JB001124, 2002b.

Fountain, A., et al.: Fractures as the main pathways of water flow in temperate glaciers, *Nature* 433, 618–621, doi:doi:10.1038/nature03296, 2005.

Goeller, S., Thoma, M., Grosfeld, K., and Miller, H.: A balanced water layer concept for subglacial hydrology in large-scale ice sheet models, *The Cryosphere*, 7, 1095–1106, 2013.

Greve, R. and Blatter, H.: *Dynamics of Ice Sheets and Glaciers*, Advances in Geophysical and Environmental Mechanics and Mathematics, Springer, 2009.

Harper, J., Bradford, J., Humphrey, N., and Meierbacholt, T.: Vertical extension of the subglacial drainage system into basal

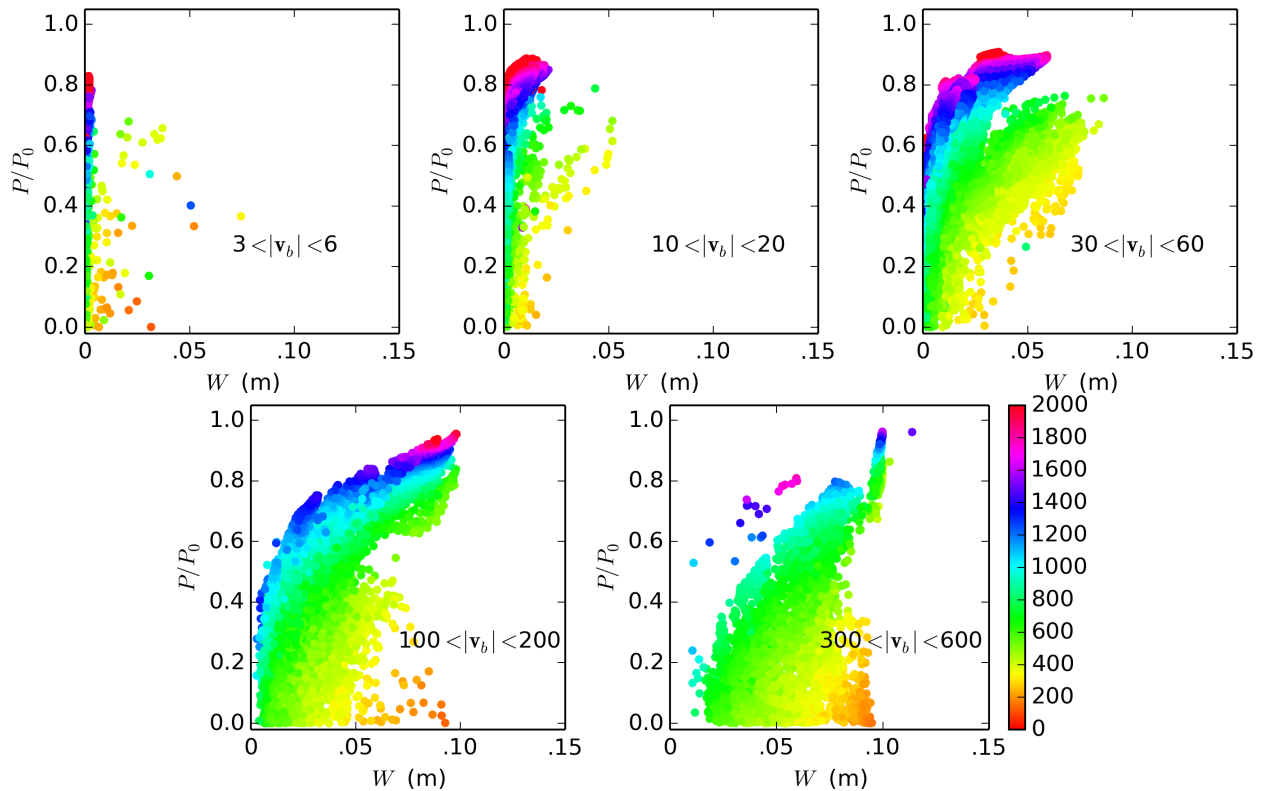


Fig. 13. Scatter plots of (W, P) pairs for all cells at end of a 5 model year steady-input simulation on a 2 km grid for the whole Greenland ice sheet using roughness scale $W_r = 0.1$ m. Each scatter plot shows the pairs for a select range of ice sliding speeds, as indicated. Points are colored by ice thickness using a common scale shown beside last figure.

- crevasses, *Nature*, 467, 579–582, doi:10.1038/nature09398,¹⁷⁸⁵ 2010.
- Hewitt, I. J.: Modelling distributed and channelized subglacial drainage: the spacing of channels, *J. Glaciol.*, 57, 302–314, 2011.
- Hewitt, I. J.: Seasonal changes in ice sheet motion due to melt water lubrication, *Earth Planet. Sci. Lett.*, 371–372, 16–25,¹⁷⁹⁰ doi:10.1016/j.epsl.2013.04.022, 2013.
- Hewitt, I. J., Schoof, C., and Werder, M. A.: Flotation and free surface flow in a model for subglacial drainage. Part II: Channel flow, *J. Fluid Mech.*, 702, 157–188, 2012.
- Hooke, R. et al.: Rheology of till beneath Störglaciären, Sweden, *J. Glaciol.*, 43, 172–179, 1997.
- Hundsdorfer, W. and Verwer, J. G.: Numerical Solution of Time-Dependent Advection-Diffusion-Reaction Equations, Springer Series in Computational Mathematics, Springer, 2010.
- Huybrechts, P. et al.: The EISMINT benchmarks for testing ice-¹⁸⁰⁰ sheet models, *Ann. Glaciol.*, 23, 1–12, 1996.
- Johnson, J. and Fastook, J. L.: Northern Hemisphere glaciation and its sensitivity to basal melt water, *Quat. Int.*, 95, 65–74, 2002.
- Kamb, B.: Glacier surge mechanism based on linked cavity configuration of the basal water conduit system, *J. Geophys. Res.*, 92,¹⁸⁰⁵ 9083–9100, 1987.
- Kamb, B.: Rheological nonlinearity and flow instability in the de-forming bed mechanism of ice stream motion, *J. Geophys. Res.: Solid Earth*, 96, 16585–16595, 1991.
- Kinderlehrer, D. and Stampacchia, G.: An Introduction to Variational Inequalities and their Applications, Pure and Applied Mathematics, Academic Press, 1980.
- Le Brocq, A., Payne, A., Siegert, M., and Alley, R.: A subglacial water-flow model for West Antarctica, *J. Glaciol.*, 55, 879–888, doi:10.3189/002214309790152564, 2009.
- LeVeque, R. J.: Finite Volume Methods for Hyperbolic Problems, Cambridge Texts in Applied Mathematics, Cambridge University Press, 2002.
- Lingle, C. S. and Brown, T. J.: A subglacial aquifer bed model and water pressure-dependent basal sliding relationship for a West Antarctic ice stream, in: Dynamics of the West Antarctic Ice Sheet, edited by der Veen, C. J. V. and Oerlemans, J., D. Reidel, 1987.
- Livingstone, S. J., Clark, C. D., Woodward, J., and Kingslake, J.: Potential subglacial lake locations and meltwater drainage pathways beneath the Antarctic and Greenland ice sheets, *The Cryosphere*, 7, 1721–1740, doi:10.5194/tc-7-1721-2013, 2013.
- Mahaffy, M. W.: A three-dimensional numerical model of ice sheets: tests on the Barnes Ice Cap, Northwest Territories, *J. Geophys. Res.*, 81, 1059–1066, 1976.
- Martin, M. A. et al.: The Potsdam Parallel Ice Sheet Model (PISM-PIK) –Part 2: Dynamic equilibrium simulation of the Antarctic ice sheet, *The Cryosphere*, 5, 727–740, 2011.
- Morton, K. W. and Mayers, D. F.: Numerical Solutions of Partial Differential Equations: An Introduction, Cambridge University Press, 2nd edn., 2005.
- Nowicki, S. et al.: Insights into spatial sensitivities of ice mass response to environmental change from the SeaRISE ice sheet

- modeling project: II. Greenland, *J. Geophys. Res.: Earth Surface*, 118, 1025–1044, doi:10.1002/jgrf.20076, 2013.
- Nye, J. F.: Water flow in glaciers: Jökulhlaups, tunnels and veins, *J. Glaciol.*, 17, 181–207, 1976.
- Pimentel, S. and Flowers, G.: A numerical study of hydrologically driven glacier dynamics and subglacial flooding, *Proc. R. Soc. A*, 467, 537–558, doi:10.1098/rspa.2010.0211, 2011.
- Pimentel, S., Flowers, G., and Schoof, C.: A hydrologically coupled higher-order flow-band model of ice dynamics with a Coulomb friction sliding law, *J. Geophys. Res.*, 115, doi:10.1029/2009JF001621, 2010.
- PISM authors: PISM, a Parallel Ice Sheet Model: User's Manual, <http://www.pism-docs.org>, 2013.
- Rooney, S. T., et al.: Till beneath ice stream B: 2. structure and continuity, *J. Geophys. Res.: Solid Earth*, 92, 8913–8920, 1987.
- Schoof, C.: The effect of cavitation on glacier sliding, *Proc. R. Soc. A*, 461, 609–627, doi:10.1098/rspa.2004.1350, 2005.
- Schoof, C.: A variational approach to ice stream flow, *J. Fluid Mech.*, 556, 227–251, 2006a.
- Schoof, C.: Variational methods for glacier flow over plastic till, *J. Fluid Mech.*, 555, 299–320, 2006b.
- Schoof, C.: Cavitation on deformable glacier beds, *SIAM J. Appl. Math.*, 67, 1633–1653, 2007.
- Schoof, C.: Coulomb friction and other sliding laws in a higher order glacier flow model, *Math. Models Methods Appl. Sci. (M3AS)*, 20, 157–189, doi:10.1142/S0218202510004180, 2010a.
- Schoof, C.: Ice sheet acceleration driven by melt supply variability, *Nature*, 468, 803–806, 2010b.
- Schoof, C., Hewitt, I. J., and Werder, M. A.: Flotation and free surface flow in a model for subglacial drainage. Part I: Distributed drainage, *J. Fluid Mech.*, 702, 126–156, 2012.
- Shreve, R.: Movement of water in glaciers, *J. Glaciol.*, 11, 205–214, 1972.
- Siegert, M., Le Brocq, A., and Payne, A.: Hydrological connections between Antarctic subglacial lakes, the flow of water beneath the East Antarctic Ice Sheet and implications for sedimentary processes, pp. 3–10, Wiley-Blackwell, 2009.
- Truffer, M. and Harrison, W.: In situ measurements of till deformation and water pressure, *J. Glaciol.*, 52, 175–182, 2006.
- Truffer, M., Echelmeyer, K., and Harrison, W.: Glacier motion dominated by processes deep in underlying till, *J. Glaciol.*, 46, 213–221, 2000.
- Truffer, M., Echelmeyer, K., and Harrison, W.: Implications of till deformation on glacier dynamics, *J. Glaciol.*, 47, 123–134, doi:10.3189/172756501781832449, 2001.
- Tulaczyk, S., Kamb, W. B., and Engelhardt, H. F.: Basal mechanics of Ice Stream B, West Antarctica 1. Till mechanics, *J. Geophys. Res.*, 105, 463–481, 2000a.
- Tulaczyk, S., Kamb, W. B., and Engelhardt, H. F.: Basal mechanics of Ice Stream B, West Antarctica 2. Undrained plastic bed model, *J. Geophys. Res.*, 105, 483–494, 2000b.
- van der Wel, N., Christoffersen, P., and Bougamont, M.: The influence of subglacial hydrology on the flow of Kamb Ice Stream, West Antarctica, *J. Geophys. Res.: Earth Surface*, 118, 1–14, doi:10.1029/2012JF002570, 2013.
- van Pelt, W.: Modelling the dynamics and boundary processes of Svalbard glaciers, Ph.D. thesis, Institute for Marine and Atmospheric Research Utrecht (IMAU), The Netherlands, 2013.
- van Pelt, W. et al.: Simulating melt, runoff and refreezing on Nordenskiöldbreen, Svalbard, using a coupled snow and energy balance model, *The Cryosphere*, 6, 641–659, doi:10.5194/tc-6-641-2012, 2012.
- Vázquez, J. L.: The Porous Medium Equation, Oxford Mathematical Monographs, The Clarendon Press Oxford University Press, Oxford, 2007.
- Walder, J. S.: Stability of sheet flow of water beneath temperate glaciers and implications for glacier surging, *J. Glaciol.*, 28, 273–293, 1982.
- Werder, M., Hewitt, I., Schoof, C., and Flowers, G.: Modeling channelized and distributed subglacial drainage in two dimensions, *J. Geophys. Res.: Earth Surface*, 118, 2140–2158, 2013.
- Wesseling, P.: Principles of Computational Fluid Dynamics, Springer-Verlag, 2001.
- Winkelmann, R. et al.: The Potsdam Parallel Ice Sheet Model (PISM-PIK) Part 1: Model description, *The Cryosphere*, 5, 715–726, 2011.